NASA TECHNICAL MEMORANDUM

NASA TM X-1848

NASA TM X-1848

CASE FILE COPY

TRANSONIC AERODYNAMIC CHARACTERISTICS OF A SATURN IB MANNED ORBITING RESEARCH LABORATORY LAUNCH VEHICLE

by Stuart G. Flechner and Richard A. Langhans

Langley Research Center
Langley Station, Hampton, Va.

NATIONAL AERONAUTICS AND SPACE ADMINISTRATION • WASHINGTON, D. C. • AUGUST 1969

1. Report No. NASA TM X-1848	2. Government Accession No.	3. Recipient's Catalog No.
4. Title and Subtitle TRANSONIC AERODYNAMIC CHARACTERISTICS OF A SATURN IB MANNED ORBITING RESEARCH LABORATORY LAUNCH VEHICLE		5. Report Date August 1969 6. Performing Organization Code
7. Author(s) By Stuart G. Flechner and Richard A. Langhans		8. Performing Organization Report No. L-6615
9. Performing Organization Name and Address NASA Langley Research Center Langley Station Hampton, Va. 23365		10. Work Unit No. 124-07-05-04-23 11. Contract or Grant No.
12. Sponsoring Agency Name and Address National Aeronautics and Space Administration Washington, D.C. 20546		13. Type of Report and Period Covered Technical Memorandum 14. Sponsoring Agency Code
15. Supplementary Notes		

16. Abstract

A wind-tunnel investigation was conducted at Mach numbers from 0.40 to 1.20, angles of attack from -6^{0} to 20^{0}, and model roll angles of 0^{0}, 45^{0}, and 90^{0} to determine the transonic aerodynamic characteristics of the Saturn IB launch vehicle with a proposed manned orbiting research laboratory (MORL). The model was tested with natural and fixed boundary-layer transition, and with and without four thrust-augmentation rockets attached to the booster. The Reynolds number, based on free-stream conditions and the first-stage diameter, varied from 0.65×10^{6} to 1.19×10^{6}.

17. Key Words Suggested by Author(s)	18. Distribution Statement
Aerodynamic characteristics Manned orbiting research laboratory (MORL) Transition effects Roll-angle effects Thrust-augmentation-rockets effects	Unclassified – Unlimited

19. Security Classif. (of this report)	20. Security Classif. (of this page)	21. No. of Pages	22. Price*
Unclassified	Unclassified	44	$3.00

*For sale by the Clearinghouse for Federal Scientific and Technical Information
Springfield, Virginia 22151

TRANSONIC AERODYNAMIC CHARACTERISTICS OF A SATURN IB MANNED ORBITING RESEARCH LABORATORY LAUNCH VEHICLE

By Stuart G. Flechner and Richard A. Langhans
Langley Research Center

SUMMARY

A wind-tunnel investigation has been conducted to determine the subsonic and transonic aerodynamic characteristics of the Saturn IB launch vehicle with a proposed manned orbiting research laboratory (MORL) payload. The model was tested with natural and fixed boundary-layer transition, and with and without thrust-augmentation rockets attached to the booster. The investigation was conducted at Mach numbers from 0.40 to 1.20, angles of attack from -6° to 20°, and roll angles of 0°, 45°, and 90°. The Reynolds number, based on free-stream conditions and the first-stage diameter, varied from 0.65×10^{6} to 1.19×10^{6}.

The results of this investigation indicate large variations in rolling moment, yawing moment, and side force for roll angles of 45° and 90° at angles of attack greater than 10°. The addition of thrust-augmentation rockets shifted the axial-force coefficient by as much as 0.20, increased the slopes of the normal-force and pitching-moment curves, and resulted in a rearward shift in the center of pressure of 1/2 a body diameter.

INTRODUCTION

The National Aeronautics and Space Administration has been conducting an investigation to determine the aerodynamic force and moment characteristics and the distribution of aerodynamic loads on a proposed manned earth-orbiting space-station booster combination. The investigation was conducted on the Saturn IB launch vehicle with the manned orbiting research laboratory (MORL) payload. This investigation was conducted to provide experimental data for trajectory analysis and stability and control studies. As part of this investigation, tests were conducted at subsonic and transonic speeds in the Langley 8-foot transonic pressure tunnel to determine the aerodynamic characteristics of the launch configuration, contained herein, and to determine the pressure distribution over the payload package. The effects of the addition of thrust-augmentation rockets and application of boundary-layer transition were also tested.

The investigation was conducted at Mach numbers from 0.40 to 1.20, angles of attack from -6° to 20°, and roll angles of 0°, 45°, and 90°. The Reynolds number, based on the first-stage diameter and free-stream conditions, varied from 0.65×10^{6} to 1.19×10^{6}.

SYMBOLS

The forces and moments measured on the vehicle were referred to the body system of coordinate axes with the origin located at engine gimbal station 100 (0.179 reference diameter forward of the model base). (See fig. 1.) The coefficients and symbols used herein are defined as follows:

A — reference area (across tanks) of 0.0132-scale model of Saturn IB launch vehicle, 58.2506 cm^2

C_A — axial-force coefficient, $\frac{\text{Axial force}}{qA}$

$C_{A,b}$ — base + cavity axial-force coefficient, $\frac{\text{Base axial force}}{qA}$

$(C_A)_{\alpha=0}$ — axial-force coefficient at $\alpha = 0^{\circ}$

$(C_{A,b})_{\alpha=0}$ — base + cavity axial-force coefficient at $\alpha = 0^{\circ}$

C_l — rolling-moment coefficient, $\frac{\text{Rolling moment}}{qAd}$

C_m — pitching-moment coefficient, $\frac{\text{Pitching moment}}{qAd}$

C_{m_α} — slope of pitching-moment-coefficient curve at $\alpha = 0^{\circ}$, $\frac{\partial C_m}{\partial \alpha}$, per deg

C_N — normal-force coefficient, $\frac{\text{Normal force}}{qA}$

C_{N_α} — slope of normal-force-coefficient curve at $\alpha = 0^{\circ}$, $\frac{\partial C_N}{\partial \alpha}$, per deg

C_n — yawing-moment coefficient, $\frac{\text{Yawing moment}}{qAd}$

C_Y — side-force coefficient, $\frac{\text{Side force}}{qA}$

d — reference diameter (across tanks) of 0.0132-scale model of Saturn IB launch vehicle, 8.6157 cm (See fig. 1(a), section A-A.)

M — free-stream Mach number

q — free-stream dynamic pressure, N/m^2

R Reynolds number based on d and free-stream conditions

r radius, cm

x_{cp}/d location of center of pressure in reference diameters forward of engine gimbal station 100 at $\alpha = 0^{o}$, $\frac{C_{m_\alpha}}{C_{N_\alpha}}$

α angle of attack, deg

ϕ angle of roll, positive clockwise as viewed from the rear of model, deg (See fig. 1(a).)

APPARATUS AND TESTS

Tunnel

The investigation was conducted in the Langley 8-foot transonic pressure tunnel. This facility is a single-return, rectangular test section, slotted-throat tunnel capable of continuous operation through the transonic speed range with negligible effects of choking and blockage.

Models

Details of the 0.0132-scale model tested are shown in figure 1, and photographs are presented in figure 2. The model was fabricated of stainless steel and designed so that the fins and thrust-augmentation rockets were interchangeable. Further details of the booster are given in reference 1. A description of each configuration is given in the following table:

Configuration	ϕ, deg	Transition	Thrust-augmentation rockets
1	0	Natural	Off
2	0	Fixed	Off
3	45	Fixed	Off
4	90	Fixed	Off
5	0	Fixed	On

Tests

Tests were conducted in the Langley 8-foot transonic pressure tunnel. The model was tested at Mach numbers from 0.40 to 1.20 at angles of attack from -6^{o} to 20^{o}. Force and moment data were obtained with an internal six-component strain-gage balance at a stagnation pressure of 1×10^5 N/m^2, a stagnation temperature of 322° K, and a dewpoint temperature such that the results were free of condensation effects. The balance remained upright as the model was rolled to obtain configurations 3 and 4. The static pressures inside the model balance cavity and at the base were measured at each test condition. The variation of test Reynolds number and dynamic pressure with Mach number is shown in figure 3.

Configurations 2, 3, 4, and 5 were tested with a boundary-layer transition strip located 2.54 cm rearward of the nose-cone tip. The strip was 0.25 cm wide and was composed of No. 100 carborundum grains (ref. 2) set in a plastic adhesive. Configuration 1 differs from configuration 2 only in its lack of a transition strip.

Corrections

The angle of attack has been corrected for tunnel flow angularity and the structural deflection of the sting-balance combination under load. At a Mach number of 1.13, a reflected shock wave passed close to the rear of the model and affected the pressures being measured there. (See fig. 4.) As a result, the summary data presented have been faired on the basis of other data in order to eliminate the apparent effect of the reflected-wave disturbance. Axial-force data presented herein have been adjusted to correspond to the condition of free-stream static pressure acting at the base of the model and in the model cavity. Plots of the axial-force-coefficient correction are given in figure 5.

Accuracy

The estimated accuracies of the data at a stagnation pressure of 1×10^5 N/m^2, based on instrument calibration and data repeatability, are within the following limits:

	M = 0.40	M = 1.20
C_N	±0.060	±0.015
C_A	±0.010	±0.003
C_m	±0.050	±0.016
C_l	±0.010	±0.003
C_n	±0.046	±0.011
C_Y	±0.035	±0.010
M	±0.003	±0.003
α, deg	±0.1	±0.1

PRESENTATION OF RESULTS

The results of this investigation are presented in the following figures:

DISCUSSION

Transition Effects

The placement of the transition strip on the nose cone had a negligible effect on both the base + cavity axial-force coefficients (fig. 5(a)) and the static aerodynamic characteristics (fig. 6) of the model. The presence of the protuberances close to the juncture of the nose cone and cylinder would be expected to cause boundary-layer transition on all configurations even for the case of no boundary-layer strips. Based upon the results of reference 3, the transition strip was assumed to be effective on this model because of its relatively small nose-cone angle. As a result, the transition strip was applied to the nose cone to determine any effects of boundary-layer conditions ahead of the protuberances.

At Mach numbers greater than 0.90, there was a slight forward shift in the center-of-pressure location x_{cp}/d. (See fig. 9(a).) The maximum shift was about 1/2 a body diameter (approximately 5 percent of the vehicle length) for configuration 1 and about 1 body diameter (10 percent) for configuration 2.

Roll-Angle Effects

Rolling the model produced significant changes in the static aerodynamic characteristics only at angles of attack greater than 10°. (See fig. 7.) At any given angle of attack, the 0° roll-angle configuration (configuration 2) had the largest normal-force, axial-force, and pitching-moment coefficients, and the 90° roll-angle configuration (configuration 4) had the least. As the model was rolled, the balance remained upright with respect to the tunnel. The rolling-moment, yawing-moment, and side-force coefficients had large variations at angles of attack greater than 10°, the 45° and 90° roll-angle configurations (configurations 3 and 4) varying more than the 0° roll-angle configuration (configuration 2).

On a slender body of revolution, which this model approximated, a pair of symmetrical vortices are formed on the lee side of the body and are discharged as a Kármán vortex street. (See ref. 4.) As the angle of attack is increased, the vortex pair becomes asymmetrical, and large variations in yawing moment and side force are produced. (See ref. 5.) After the vortices become asymmetrical, they may also become aperiodic; that is, the vortex closest to the body may first be on one side and then on the other, this switching being irregular. (See ref. 6.) References 7 and 8 also describe this phenomenon and, in addition, present applicable schlieren photographs and data.

The model was not symmetrical in the pitch plane, but the lee side (for $\alpha > 0^{\circ}$) of configuration 2 was symmetrical. Configurations 3 and 4 each had an asymmetrical (with respect to the pitch plane) protuberance on the lee side of the payload (MORL). Thus the vortices formed by configuration 2 should have remained symmetrical to larger angles of attack than those formed by configurations 3 and 4. The asymmetrical protuberances helped to make the vortices asymmetric at smaller angles of attack. This feature resulted in much lower variations in yawing-moment and side-force coefficients for configuration 2. (See figs. 7(e) and 7(f).) The asymmetric vortices also created asymmetric loading of the fins, and this loading produced larger variation in rolling-moment coefficients (fig. 7(d)) for configurations 3 and 4 than for configuration 2.

The air flow coming around the side of the model produced a force on the protuberances. The protuberances on the sides of the model had the largest forces exerted on them; and therefore, configuration 2, with the large protuberances on its sides, had the largest normal-force and pitching-moment coefficients at large angles of attack. (See figs. 7(a) and 7(c).)

Thrust-Augmentation-Rockets Effects

As to be expected, replacing the horizontal and vertical fins with four thrust-augmentation rockets produced an incremental increase in the axial-force coefficient. This increment was 0.15 or less for Mach numbers less than 0.90 and approximately 0.20 for Mach numbers greater than 0.90 at $\alpha = 0^{\circ}$. (See figs. 8(b) and 9(d).)

The slopes of the normal-force and pitching-moment coefficients (figs. 8(a), 8(c), and 9(c)), became more positive because of the additional loading area available with the rockets on. As with the other configurations, at Mach numbers greater than 0.90, the center-of-pressure location (fig. 9(c)) shifted forward about 1 body diameter. Also the addition of the rockets (configuration 5) shifted the center-of-pressure location, at each Mach number, rearward about 1/2 a body diameter (5 percent of the vehicle length) compared with configuration 2.

CONCLUDING REMARKS

A wind-tunnel investigation has been conducted to determine the subsonic and transonic aerodynamic characteristics of a manned orbiting research laboratory (MORL) payload in combination with the Saturn IB launch vehicle with and without thrust-augmentation rockets. The investigation was conducted at Mach numbers from 0.40 to 1.20, angles of attack from -6° to 20°, and roll angles of 0°, 45°, and 90°.

The results of the investigation indicate that for angles of attack greater than 10°, the 45° and 90° roll-angle configurations experienced large variations in rolling-moment, yawing-moment, and side-force coefficients. These variations were due to the formation of vortices on the body.

The addition of thrust-augmentation rockets appreciably affected the aerodynamic characteristics of the launch configuration. Axial-force coefficient shifted as much as 0.20, slopes of normal-force and pitching-moment curves became more positive, and the center of pressure moved rearward 1/2 a body diameter (5 percent of the vehicle length).

Langley Research Center,
National Aeronautics and Space Administration,
Langley Station, Hampton, Va., May 21, 1969,
124-07-05-04-23.

REFERENCES

1. Carter, C. Robert: Transonic Aerodynamic Characteristics of a Saturn IB-Apollo Launch Vehicle With Various Upper-Stage Configurations. NASA TN D-2829, 1965.
2. Braslow, Albert L.; and Knox, Eugene C.: Simplified Method for Determination of Critical Height of Distributed Roughness Particles for Boundary-Layer Transition at Mach Numbers From 0 to 5. NACA TN 4363, 1958.
3. Kelly, Thomas C.: A Transonic Investigation of Base Pressures Associated With Shallow Three-Dimensional Rearward-Facing Steps. NASA TN D-2927, 1965.
4. Allen, H. Julian; and Perkins, Edward W.: A Study of Effects of Viscosity on Flow Over Slender Inclined Bodies of Revolution. NACA Rep. 1048, 1951. (Supersedes NACA TN 2044.)
5. Letko, William: A Low-Speed Experimental Study of the Directional Characteristics of a Sharp-Nosed Fuselage Through a Large Angle-of-Attack Range at Zero Angle of Sideslip. NACA TN 2911, 1953.
6. Dunn, Eldon L.: A Low-Speed Experimental Study of Yaw Forces on Bodies of Revolution at Large Angles of Pitch and Zero Angle of Sideslip. TM-1588, U.S. Naval Ord. Test Station, Mar. 8, 1954.
7. Raney, D. J.: Measurement of the Cross Flow Around an Inclined Body at a Mach Number of 1.91. Tech. Note No. Aero 2357, Brit. R.A.E., Jan. 1955.
8. Ferris, James C.: Static Stability Investigation of a Single-Stage Sounding Rocket at Mach Numbers From 0.60 to 1.20. NASA TN D-4013, 1967.

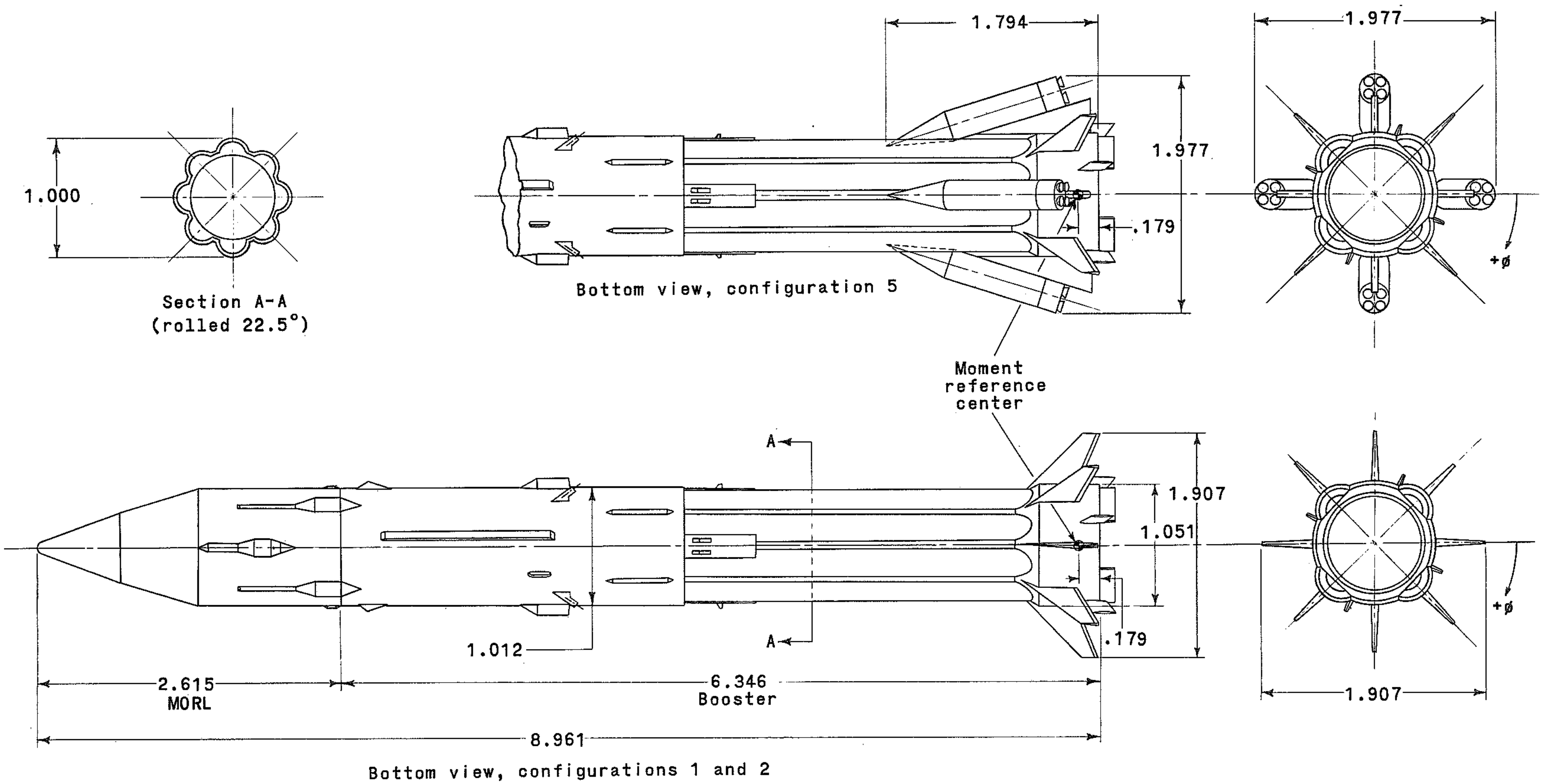

(a) Overall details.

Figure 1.- Model geometric details. All dimensions are in terms of the diameter across the booster tanks, 8.6157 cm.

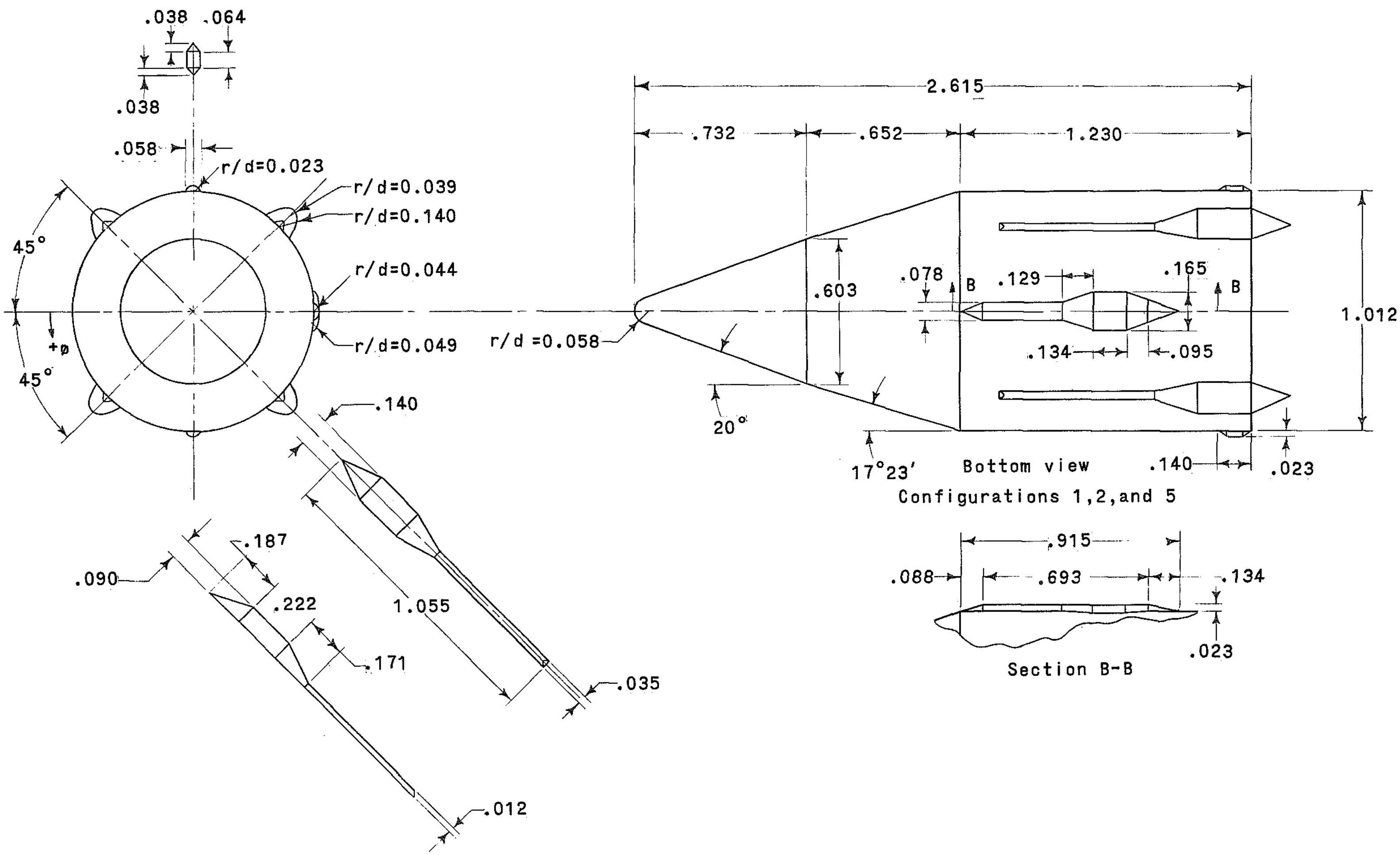

(b) MORL details.

Figure 1.- Continued.

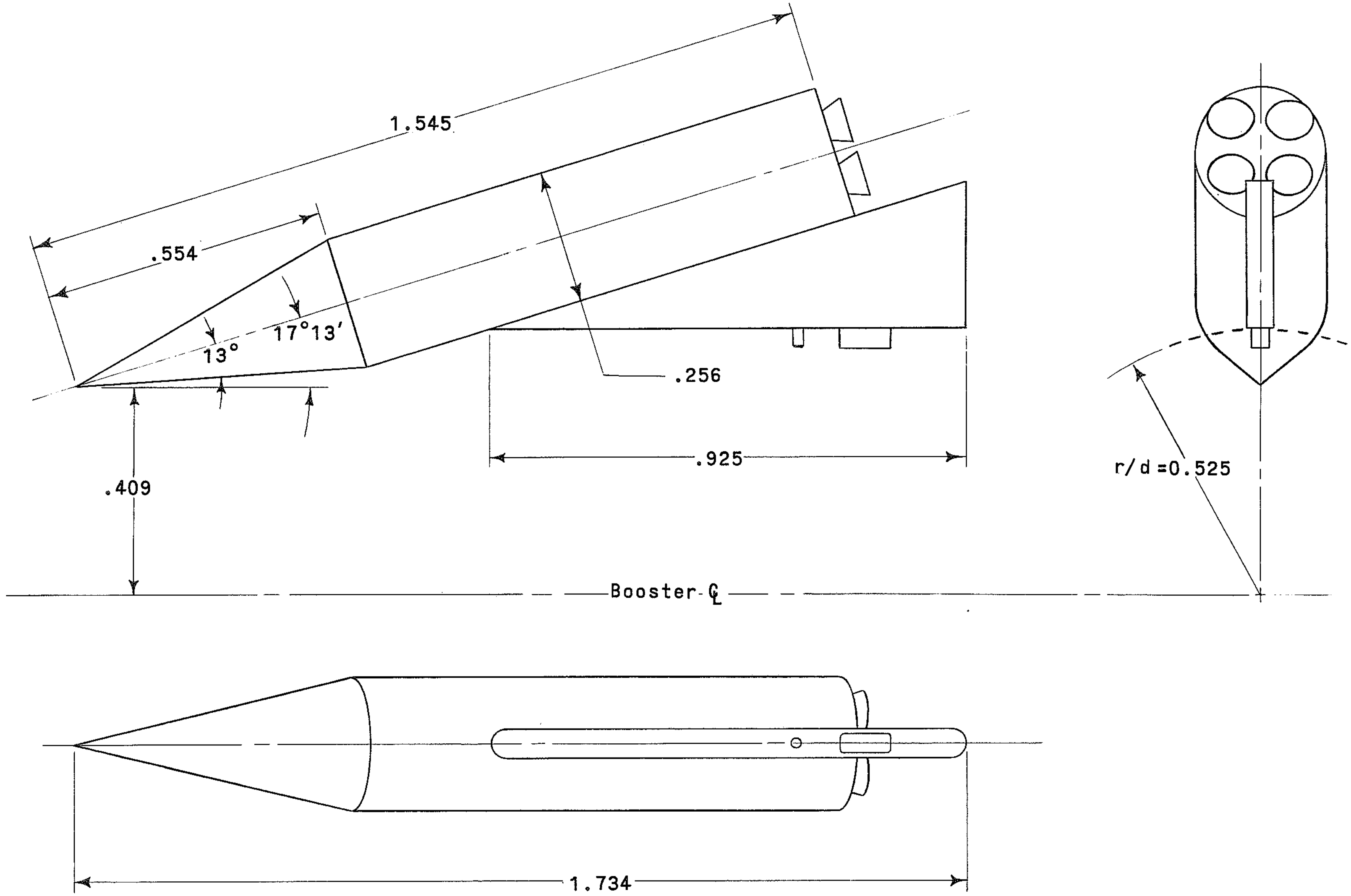

(c) Thrust-augmentation-rocket details.

Figure 1.- Concluded.

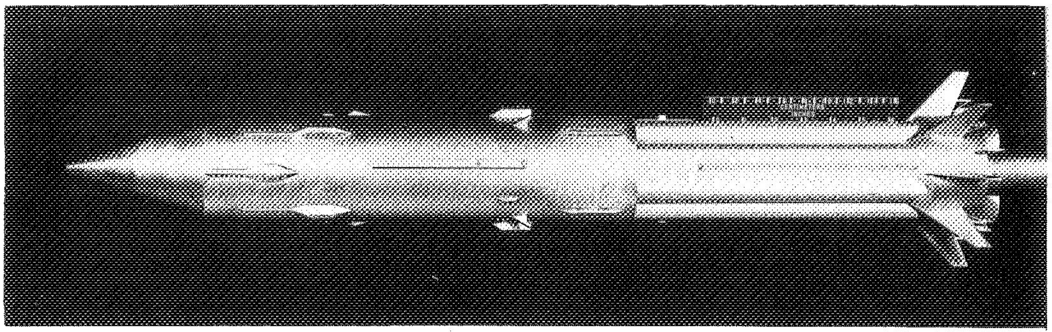

(a) Configuration 1. L-66-7921

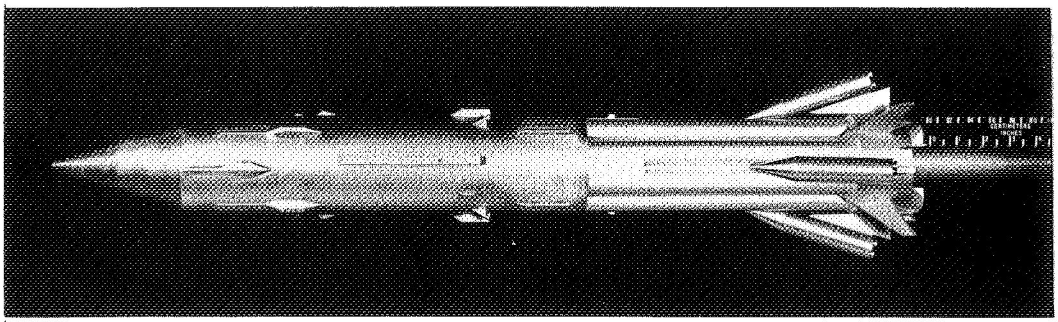

(b) Configuration 5. L-66-7920

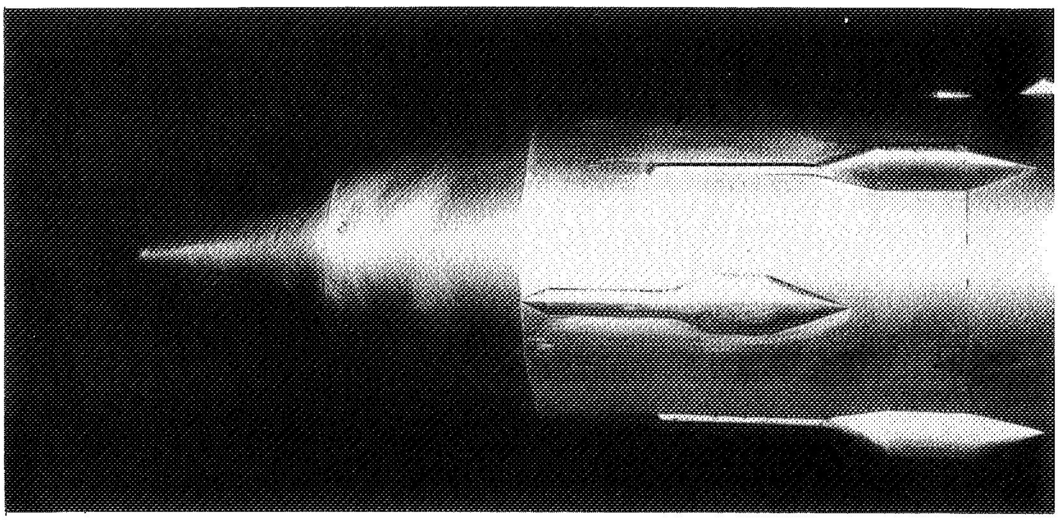

(c) MORL. L-66-7922

Figure 2.- Photographs of model as viewed from floor of wind tunnel.

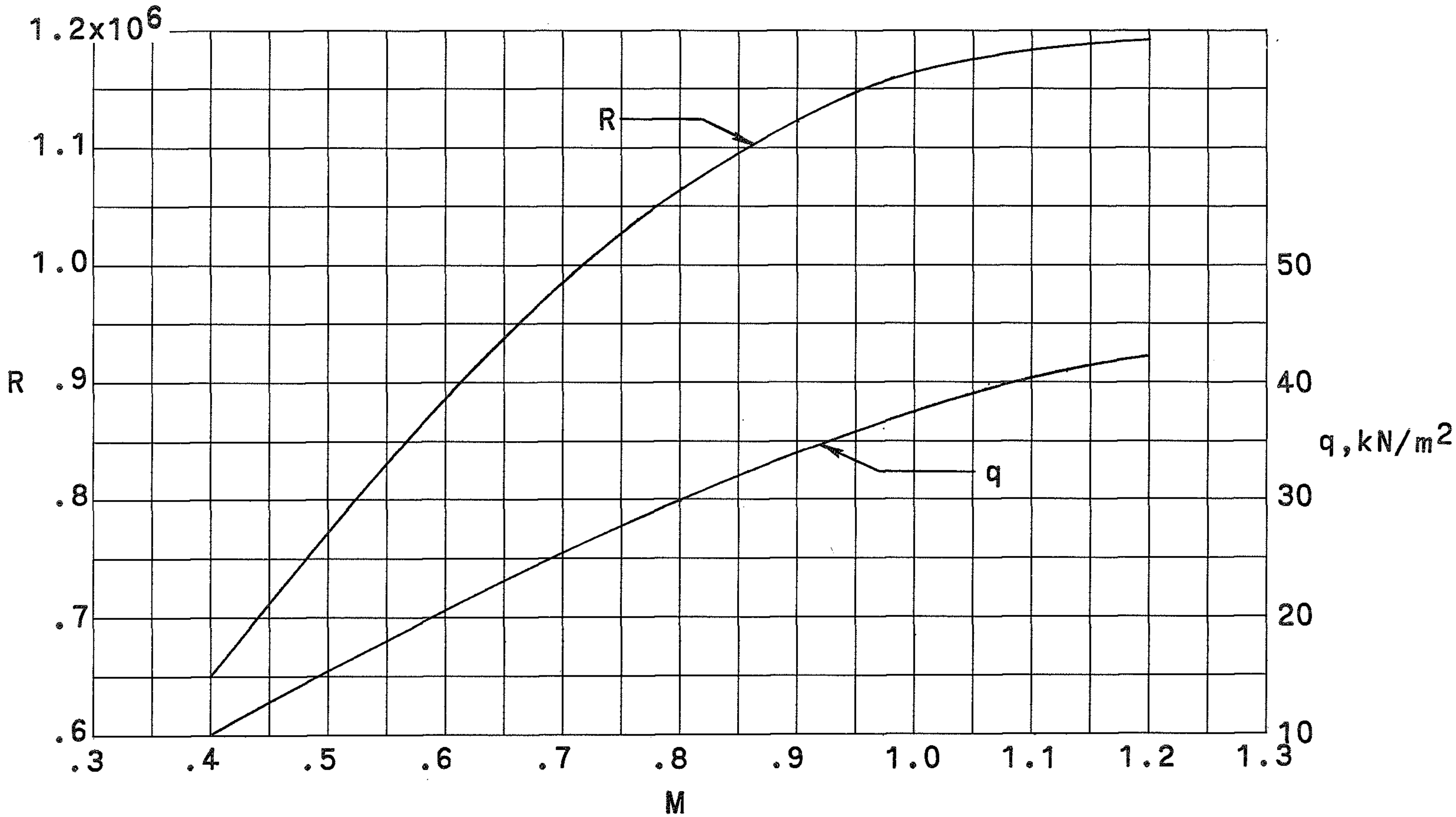

Figure 3.- Variation of test Reynolds number, based on a model diameter of 8.6157 cm, and dynamic pressure with Mach number.

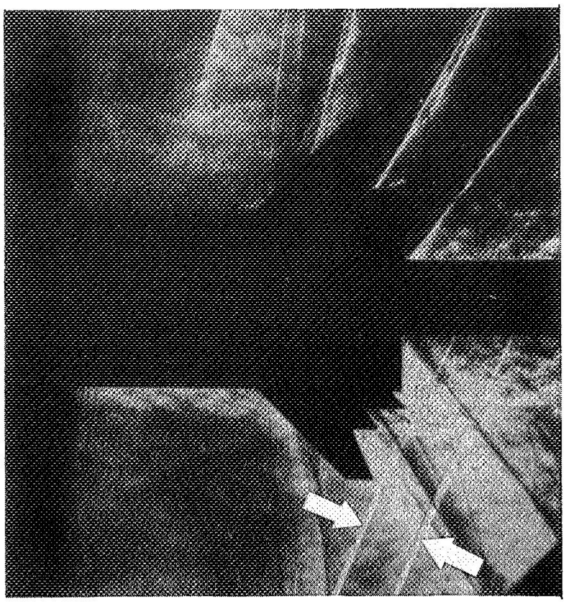

α=0°,M=1.13

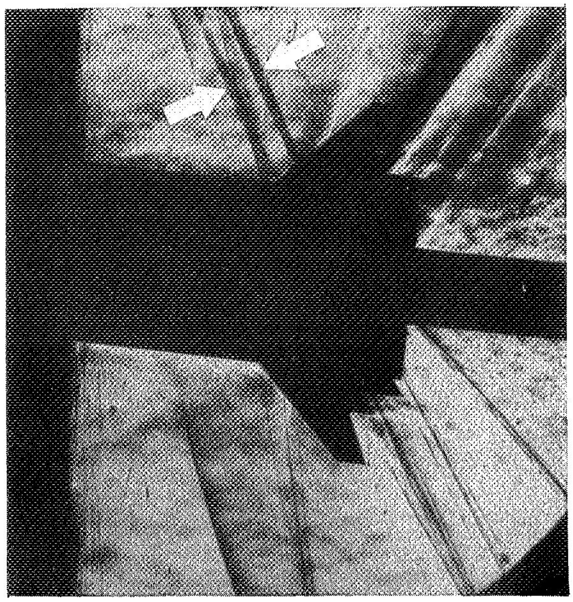

α=6°,M=1.13

(a) Reflected shock wave (arrows).

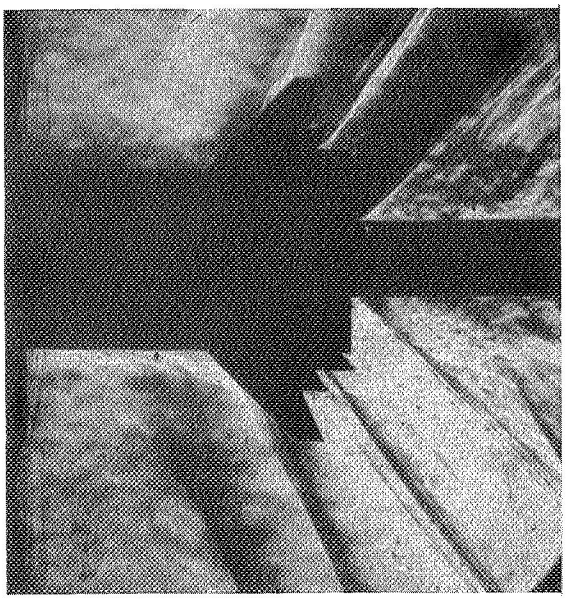

α=0°,M=1.20

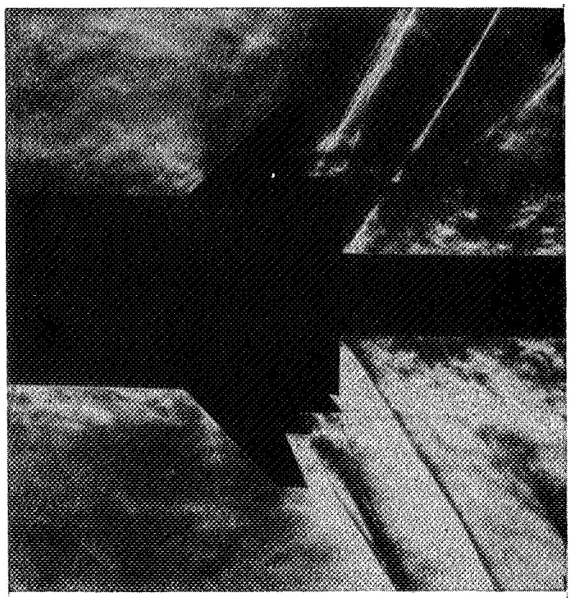

α=0°,M=1.00

(b) No reflected shock wave.

Figure 4.- Schlieren photographs showing shock waves in vicinity of model base. Configuration 2. L-69-5213

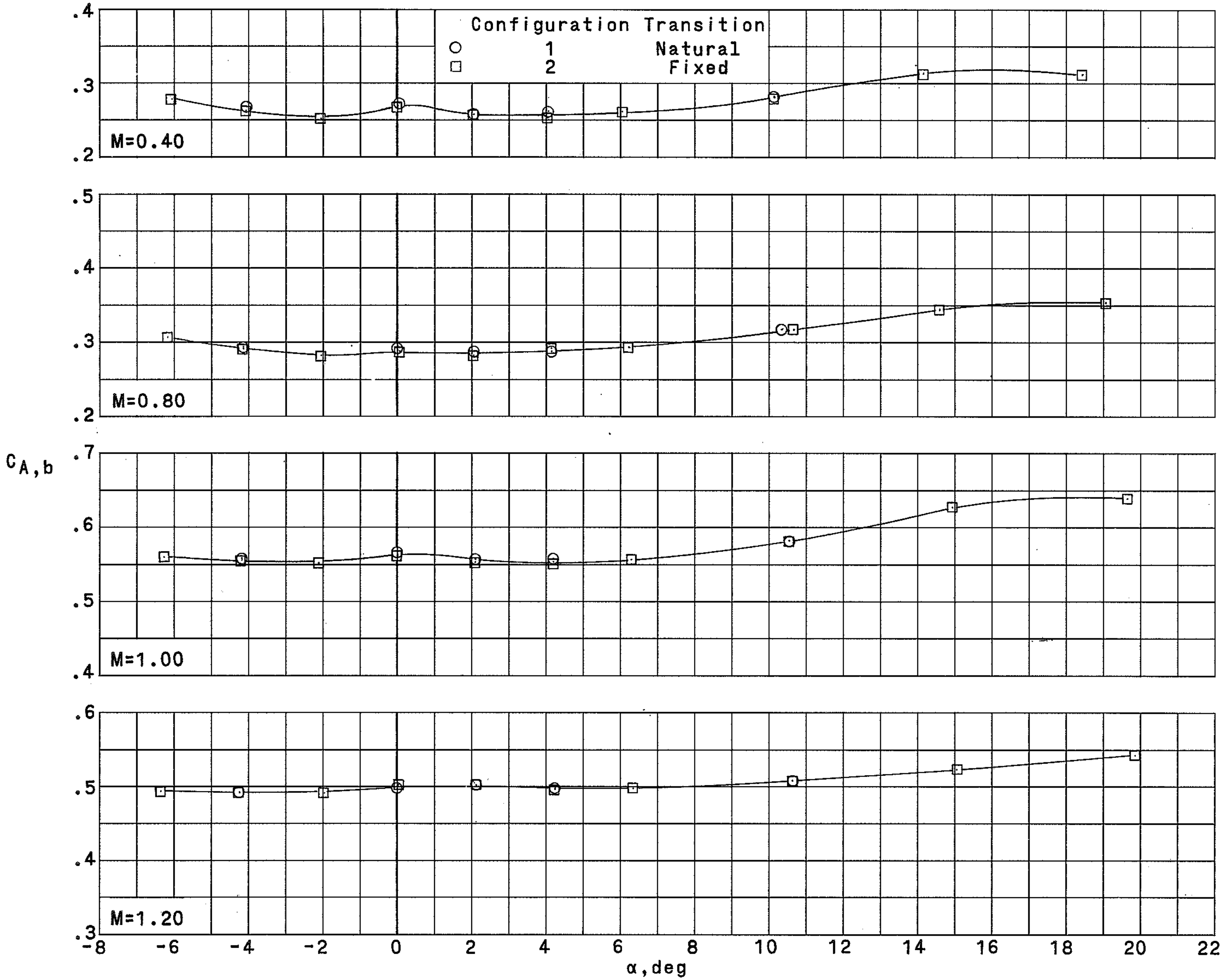

(a) Configurations 1 and 2. Transition effects.

Figure 5.- Variation of base + cavity axial-force coefficient with angle of attack.

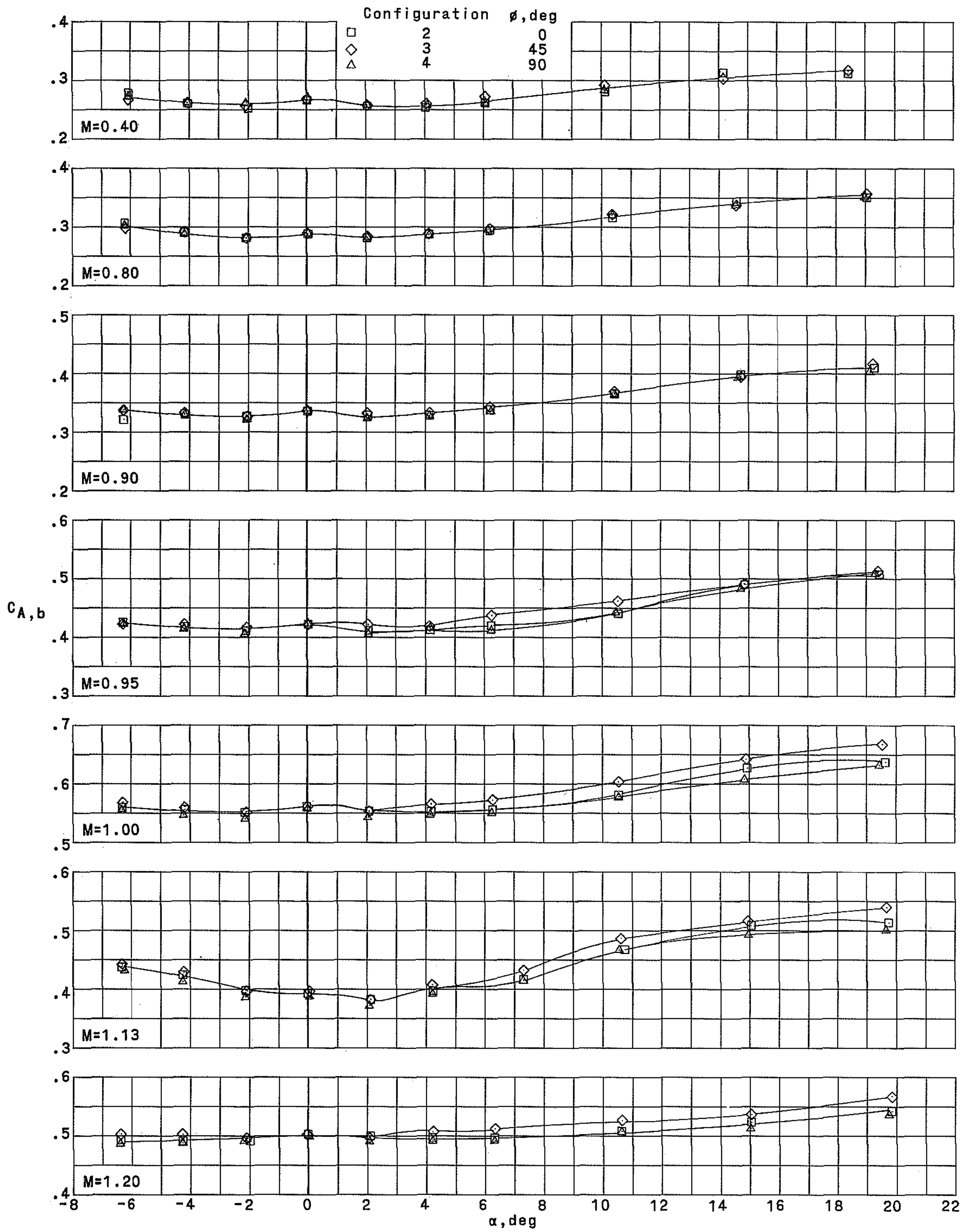

(b) Configurations 2, 3, and 4. Roll-angle effects.

Figure 5.- Continued.

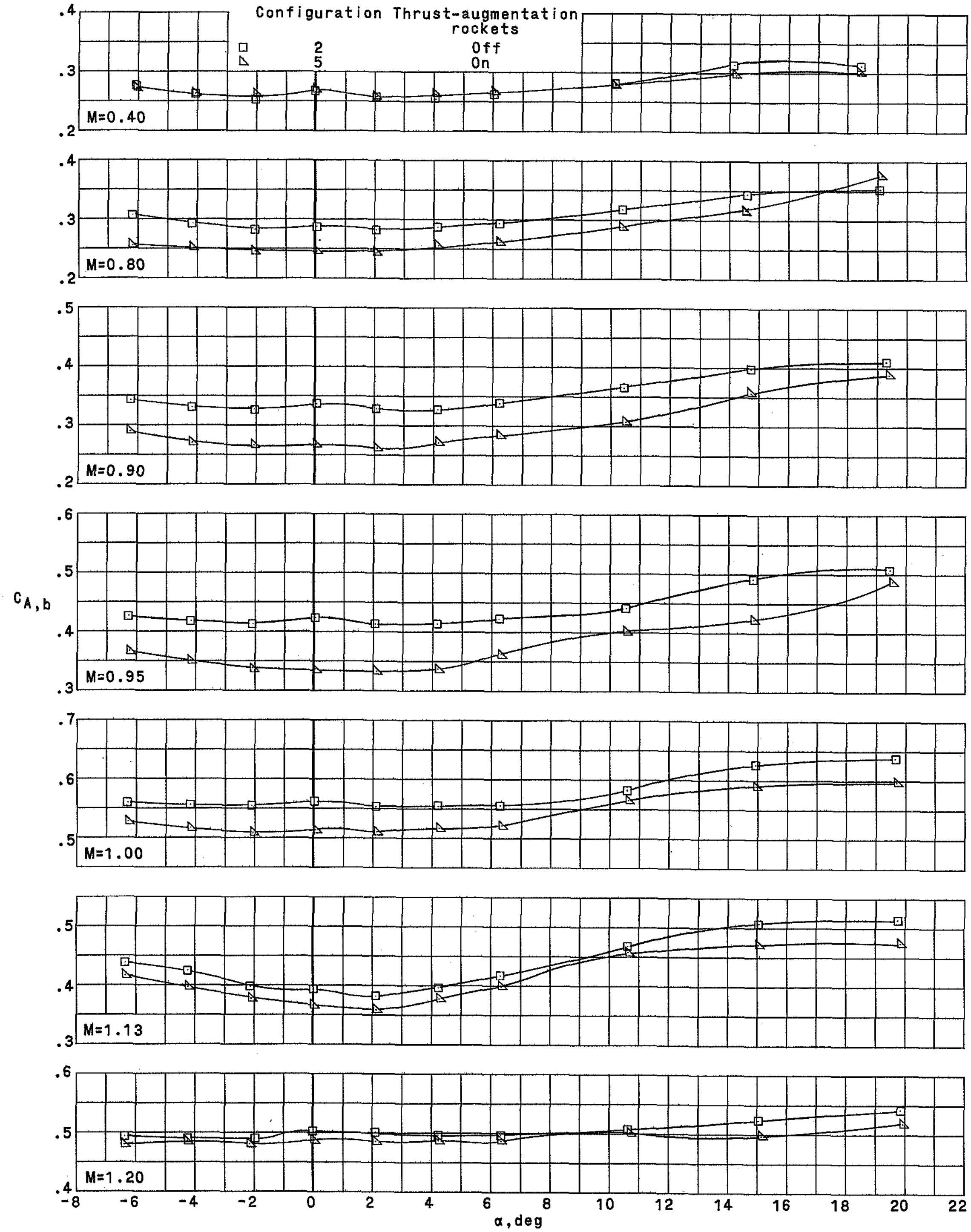

(c) Configurations 2 and 5. Thrust-augmentation-rockets effects.

Figure 5.- Concluded.

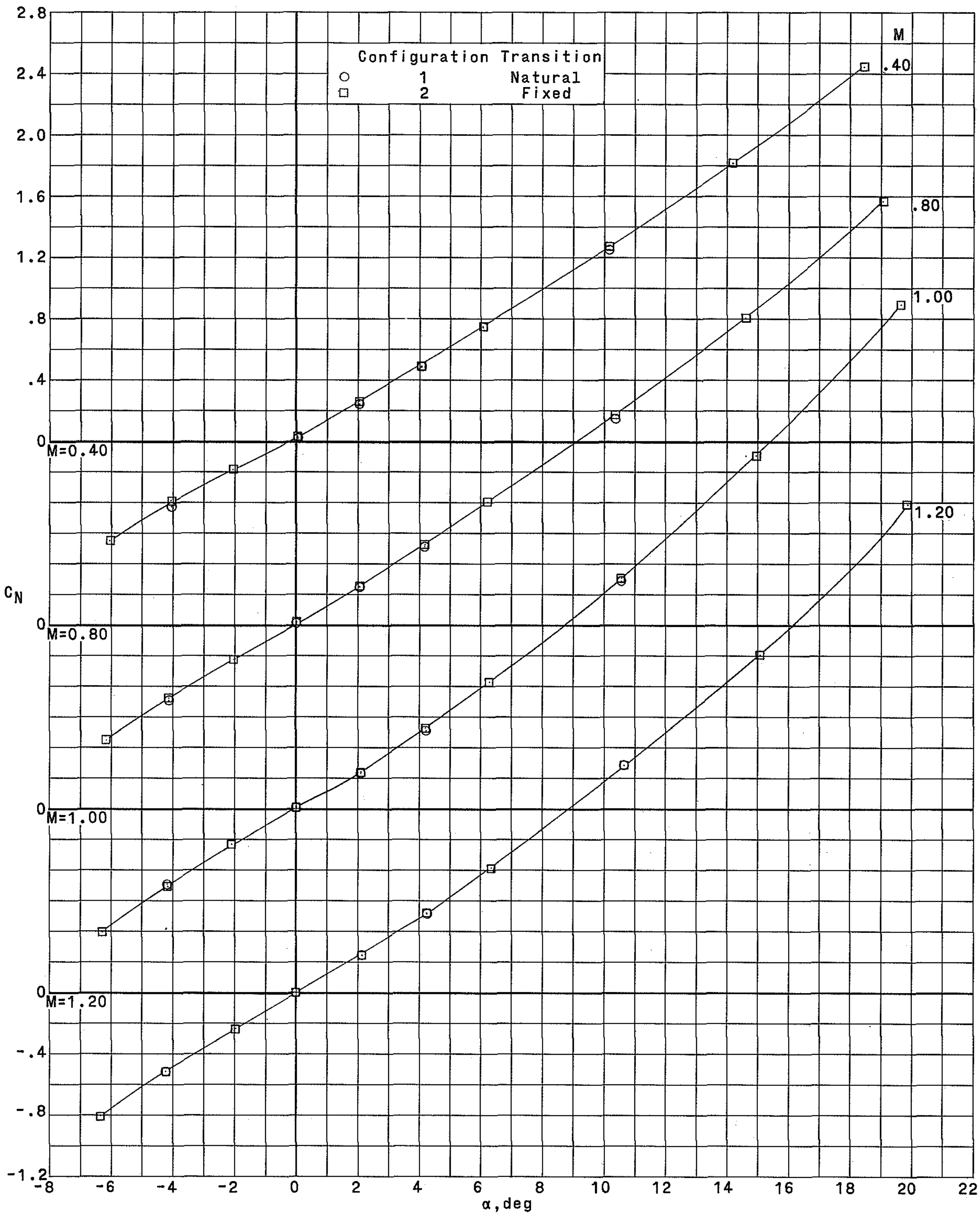

(a) Normal-force coefficient.

Figure 6.- Static aerodynamic characteristics of configurations 1 and 2. Transition effects.

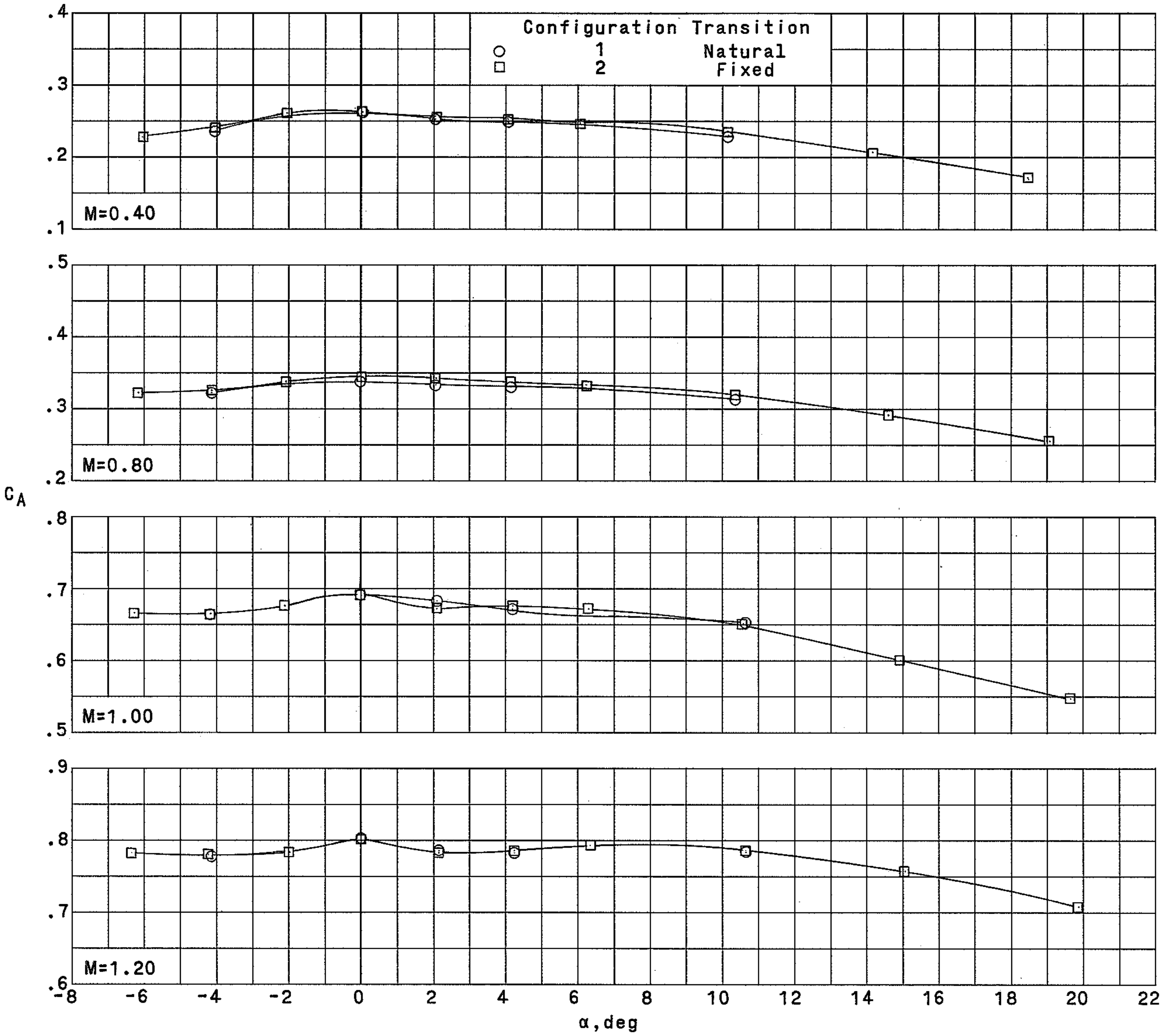

(b) Axial-force coefficient.

Figure 6.- Continued.

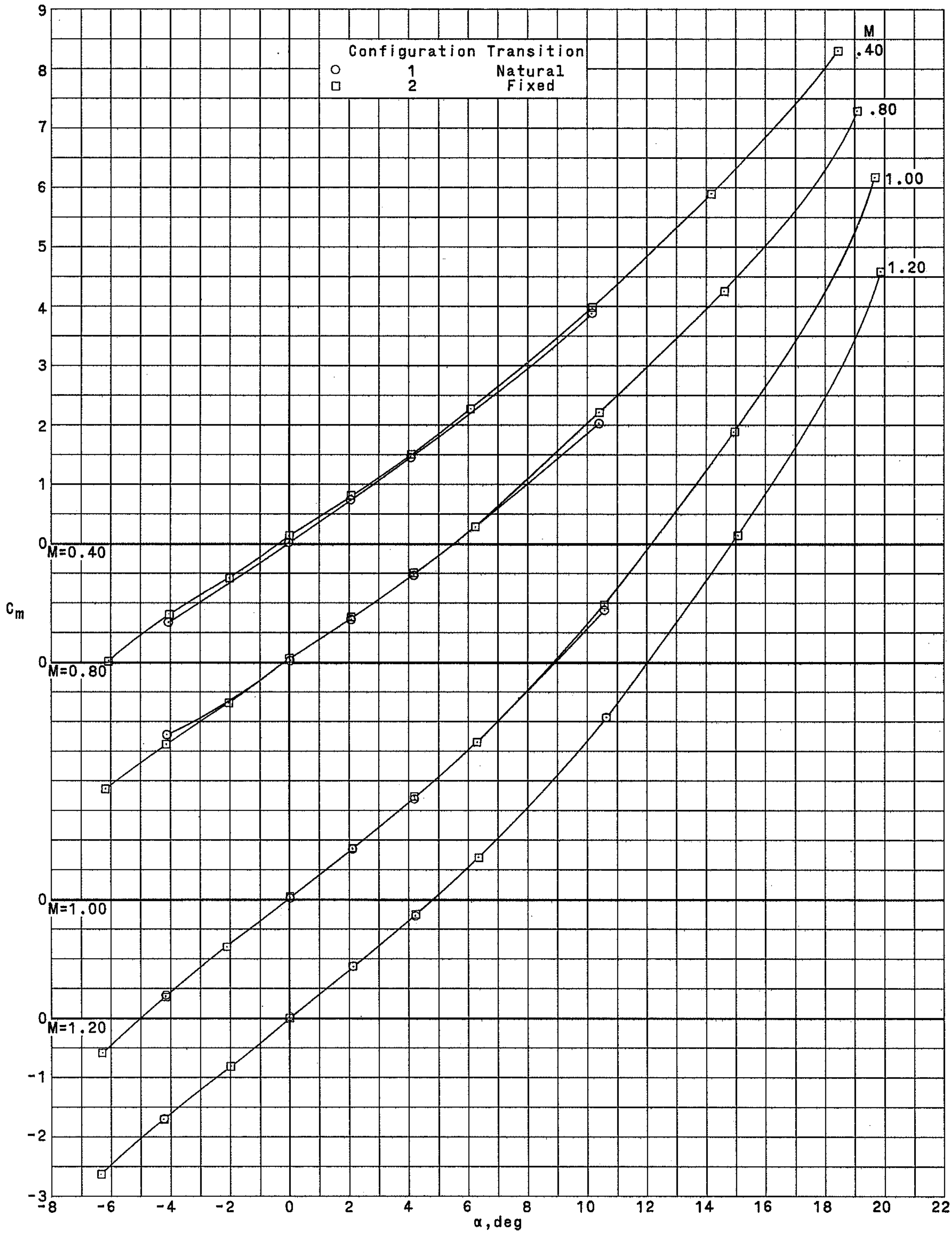

(c) Pitching-moment coefficient.

Figure 6.- Continued.

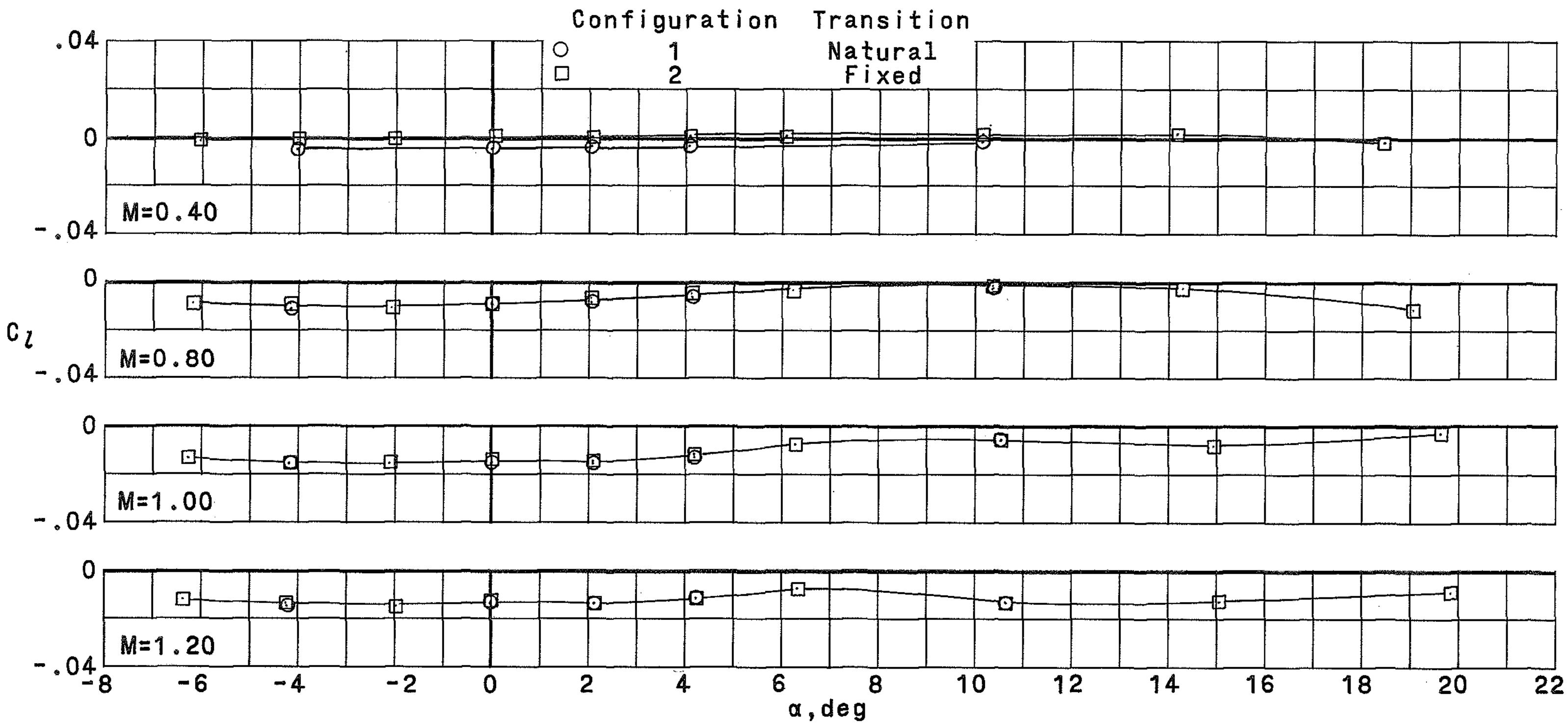

(d) Rolling-moment coefficient.

Figure 6.- Continued.

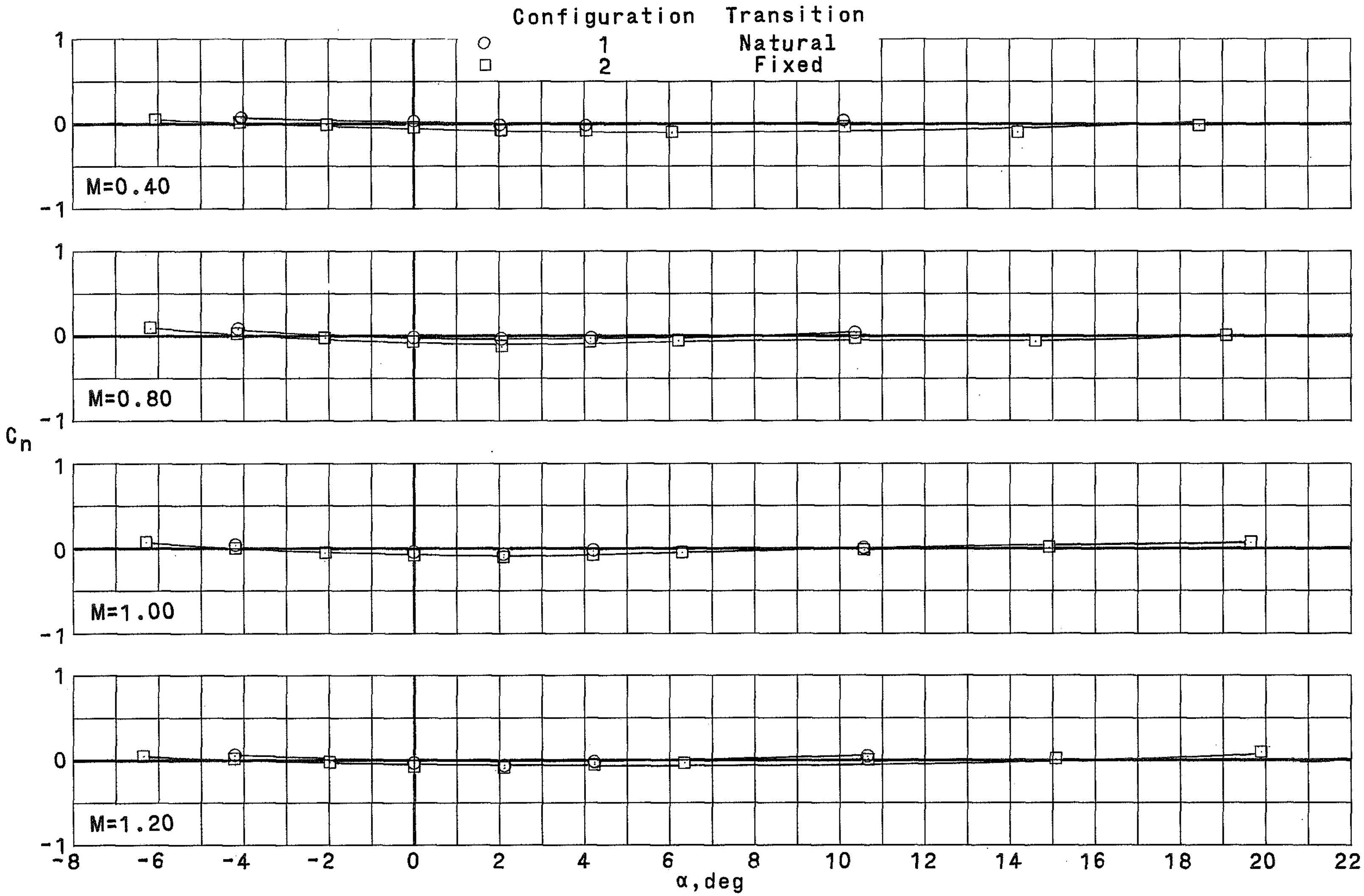

(e) Yawing-moment coefficient.

Figure 6.- Continued.

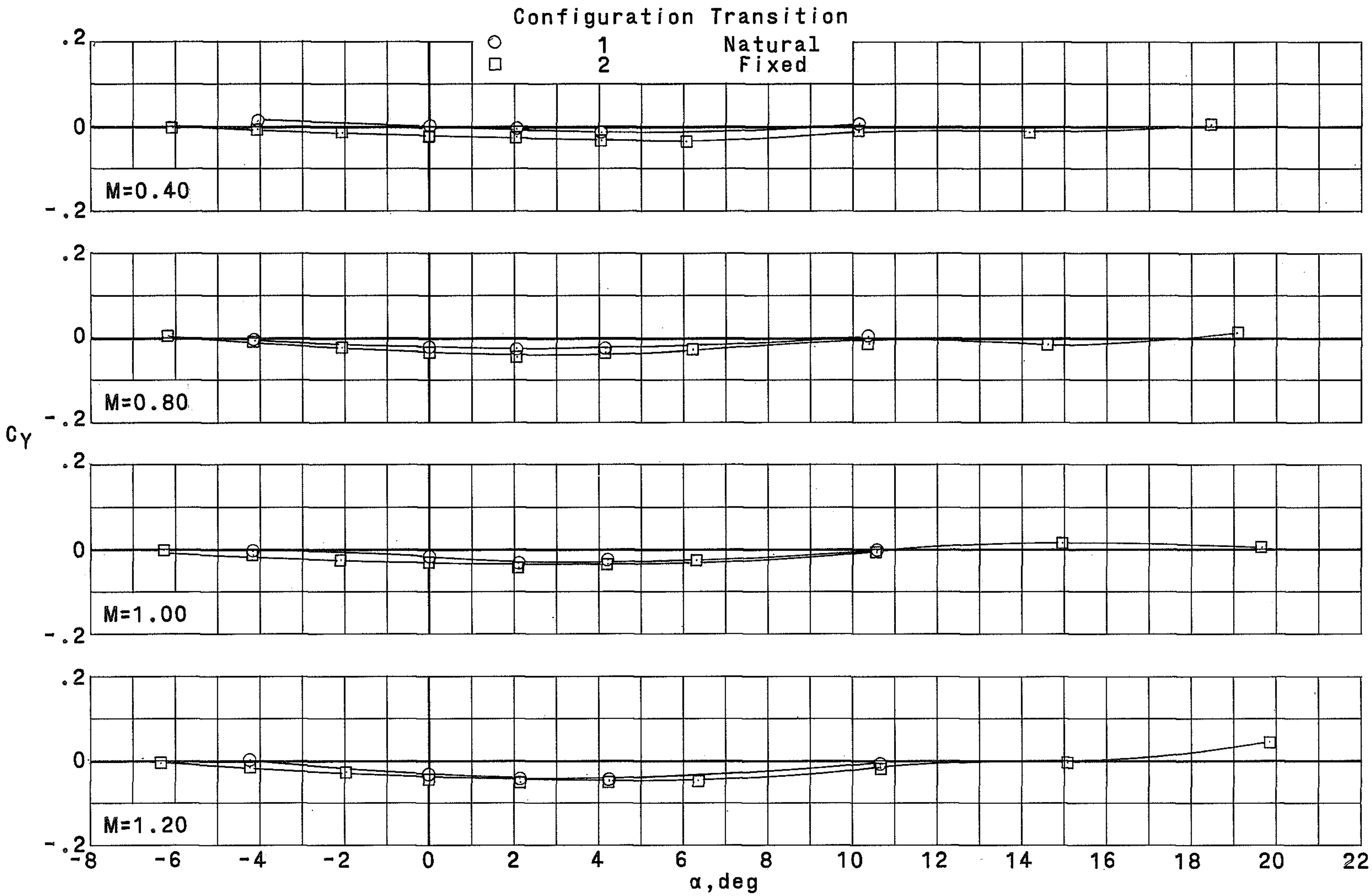

(f) Side-force coefficient.

Figure 6.- Concluded.

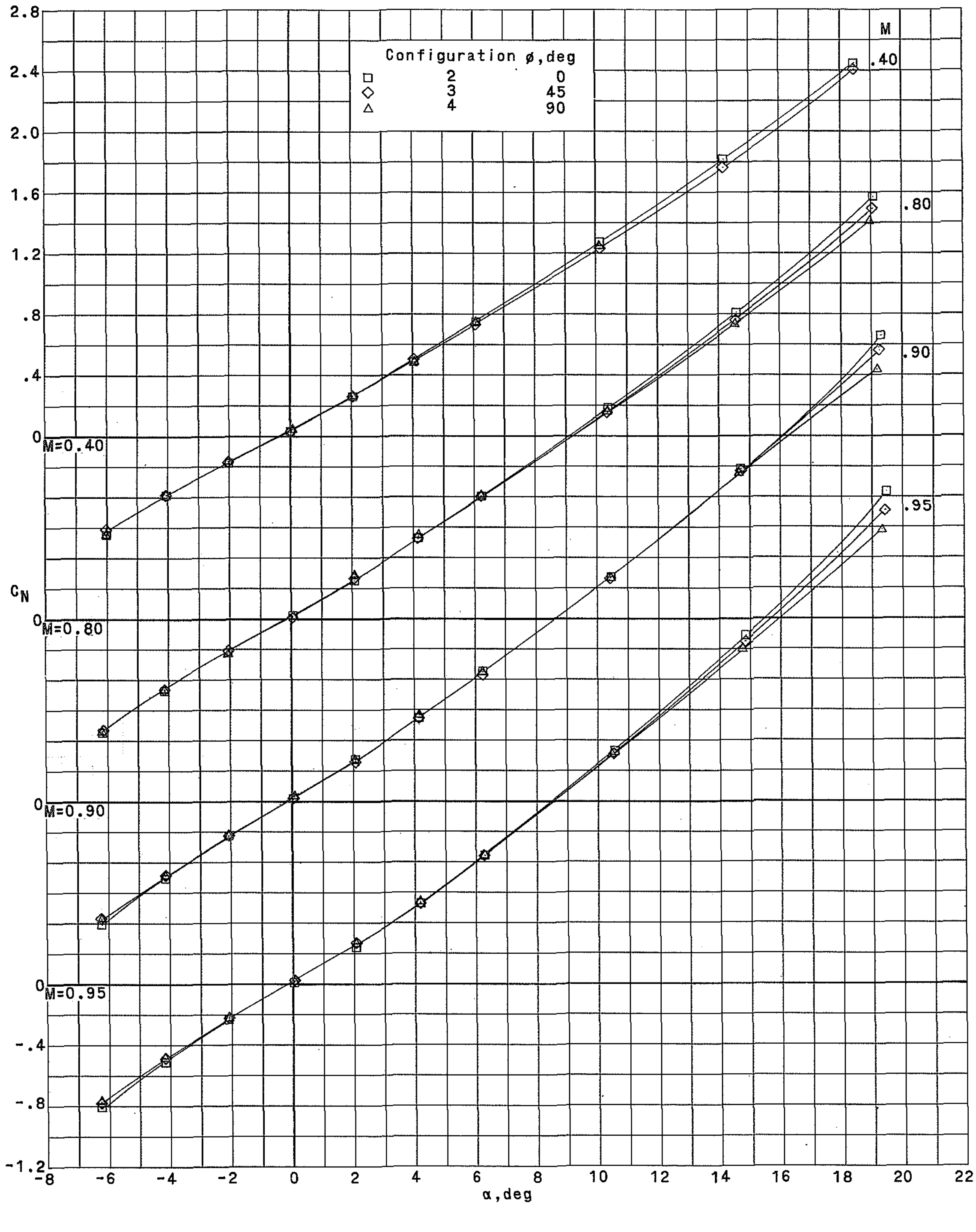

(a) Normal-force coefficient.

Figure 7.- Static aerodynamic characteristics of configurations 2, 3, and 4. Roll-angle effects.

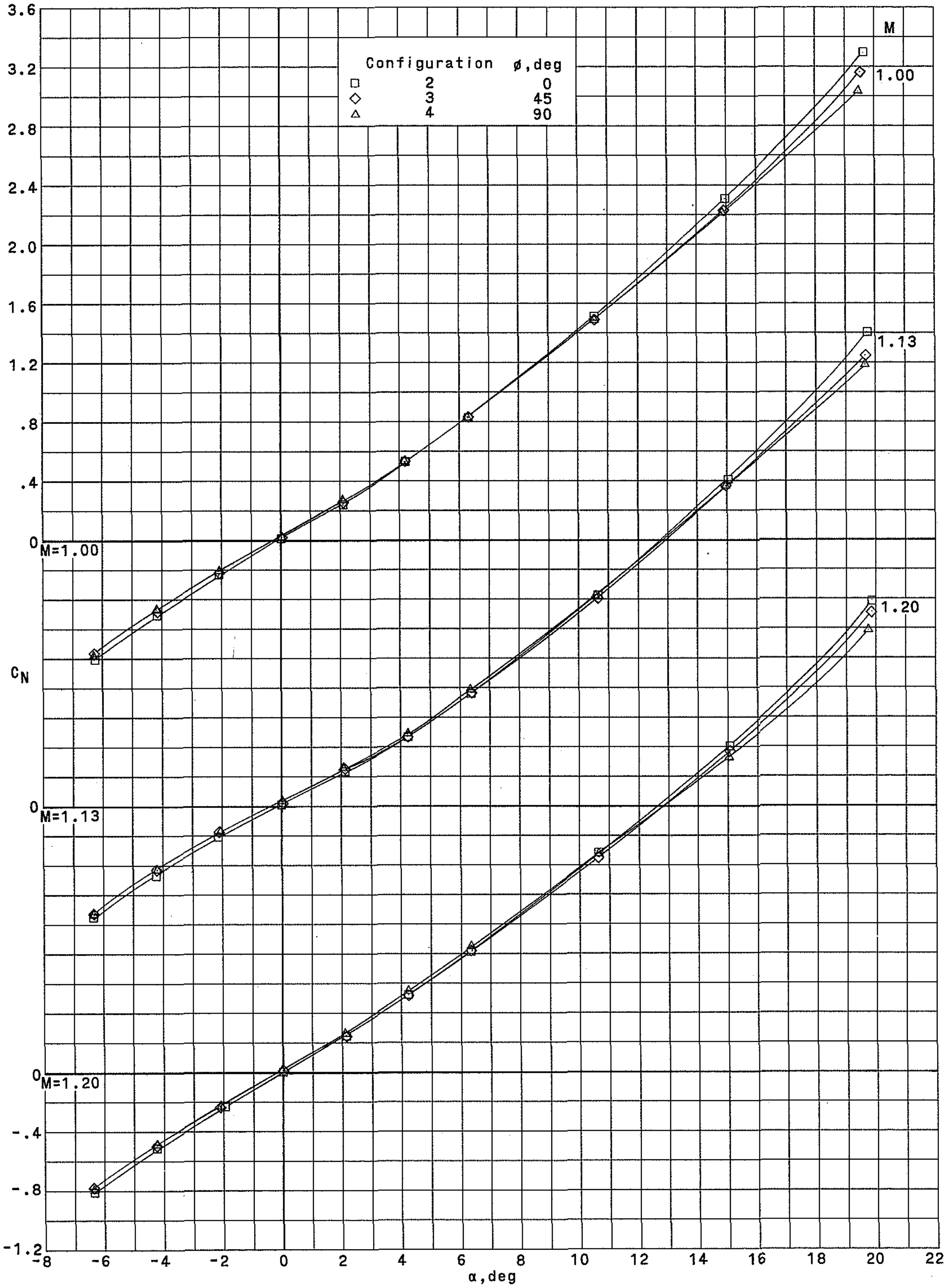

(a) Normal-force coefficient. Concluded.

Figure 7.- Continued.

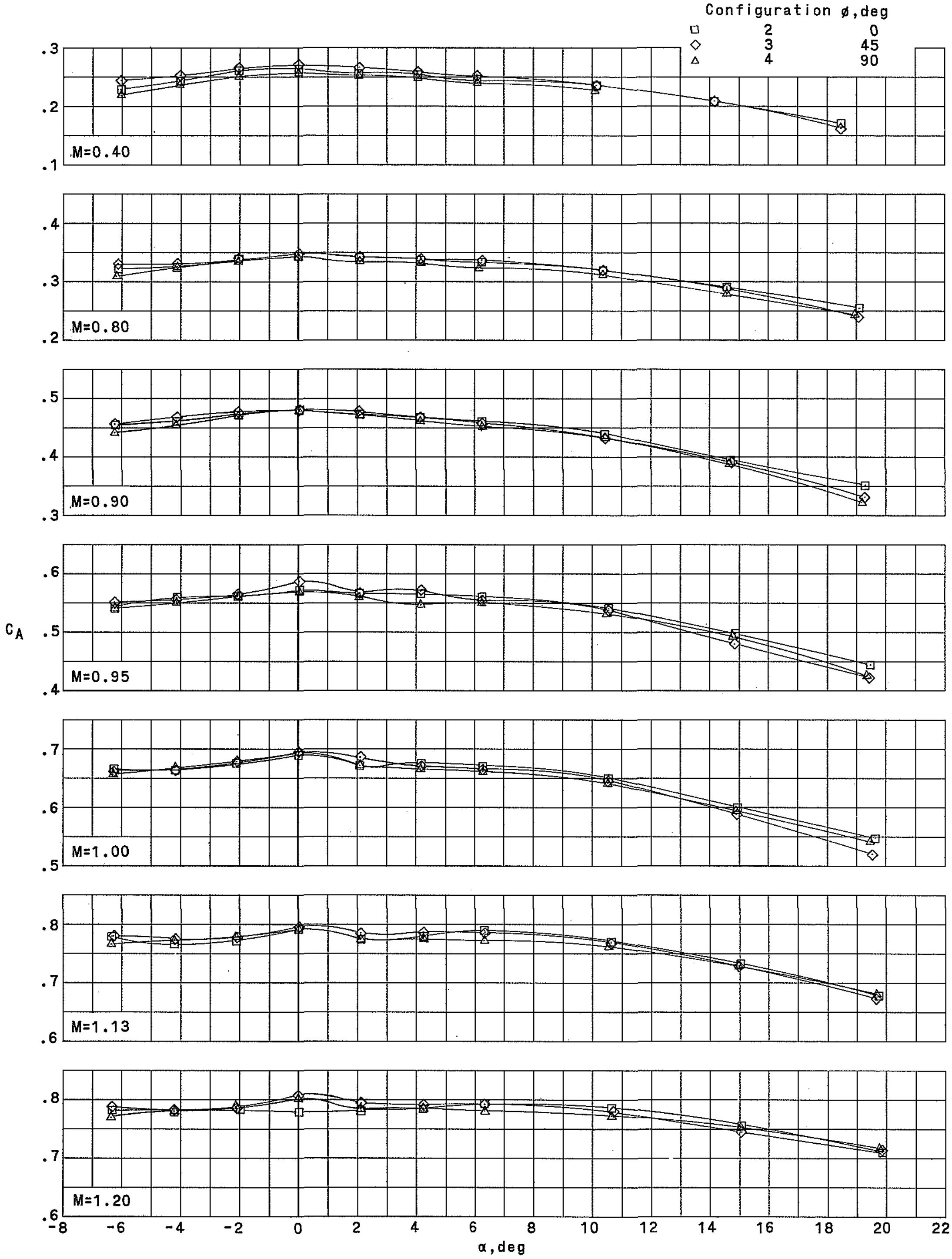

(b) Axial-force coefficient.

Figure 7.- Continued.

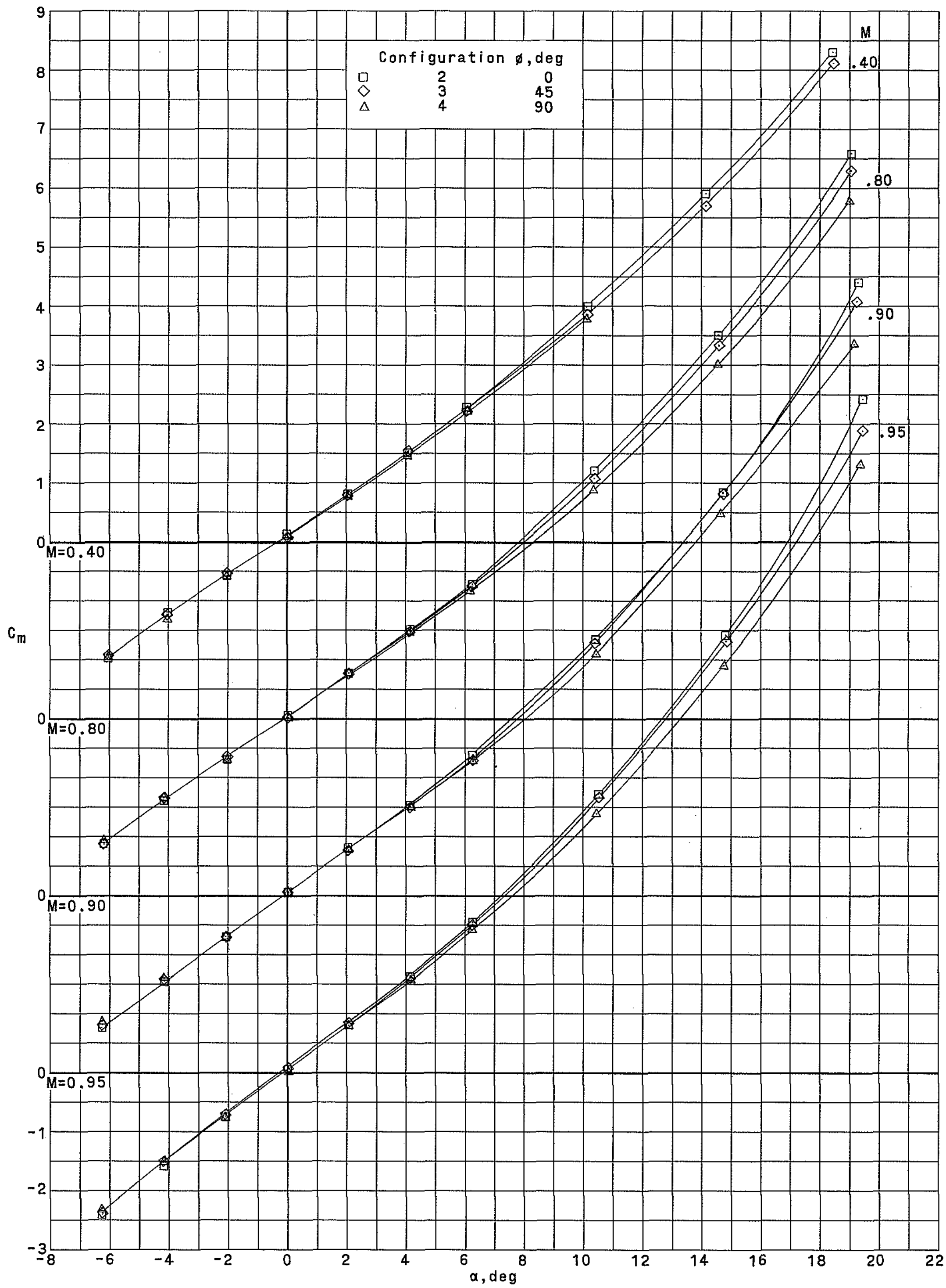

(c) Pitching-moment coefficient.

Figure 7.- Continued.

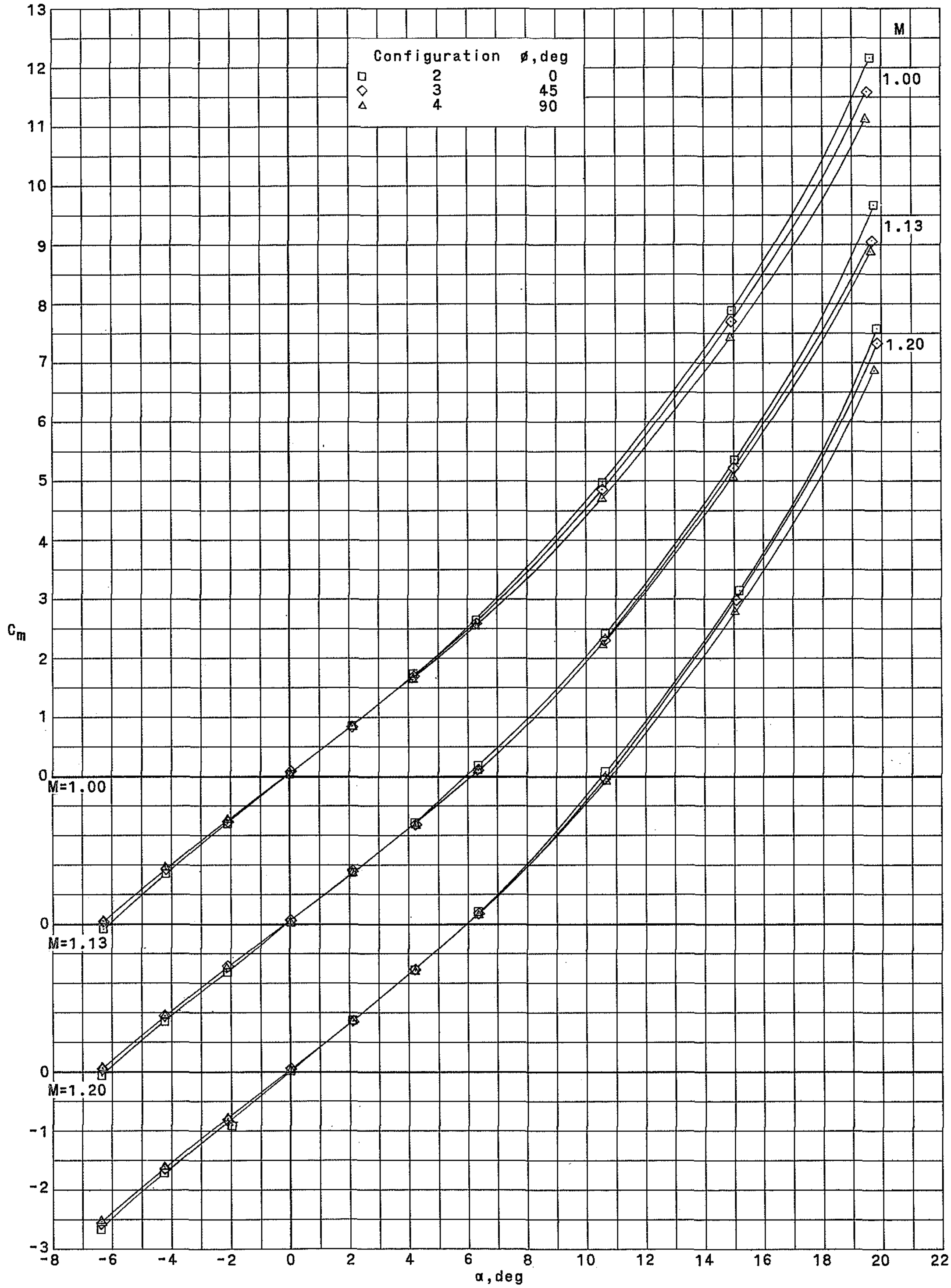

(c) Pitching-moment coefficient. Concluded.

Figure 7.- Continued.

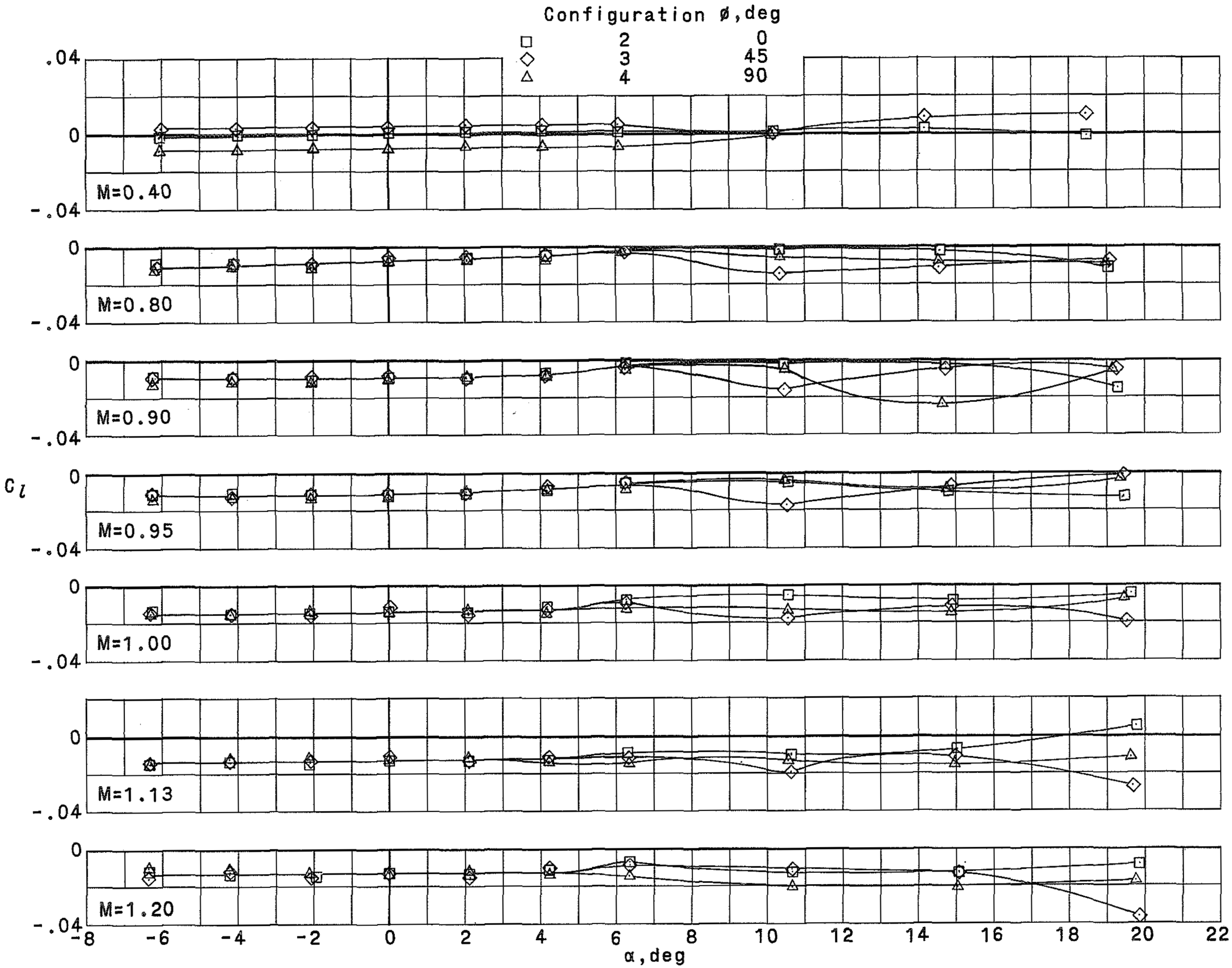

(d) Rolling-moment coefficient.

Figure 7.- Continued.

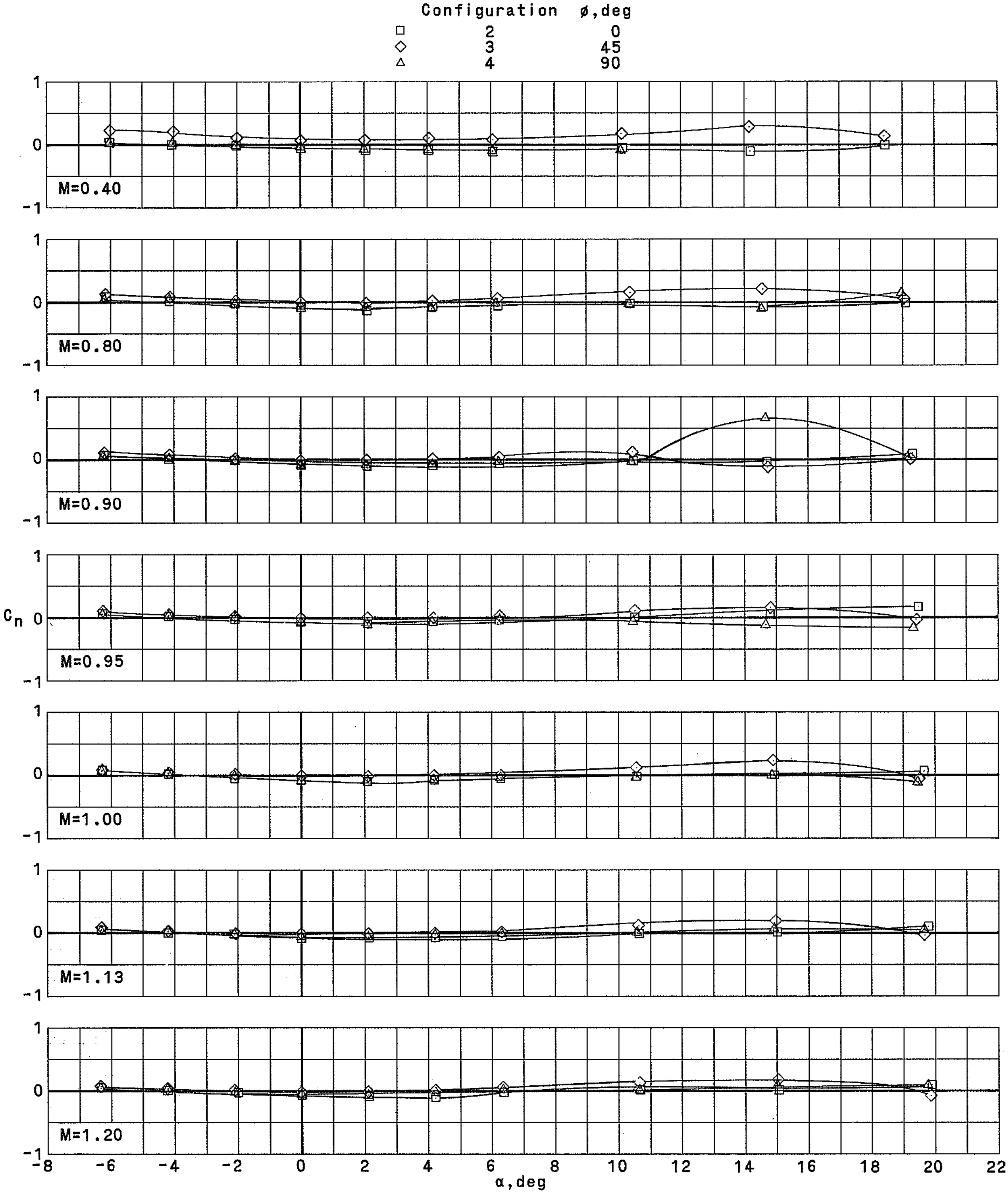

(e) Yawing-moment coefficient.

Figure 7.- Continued.

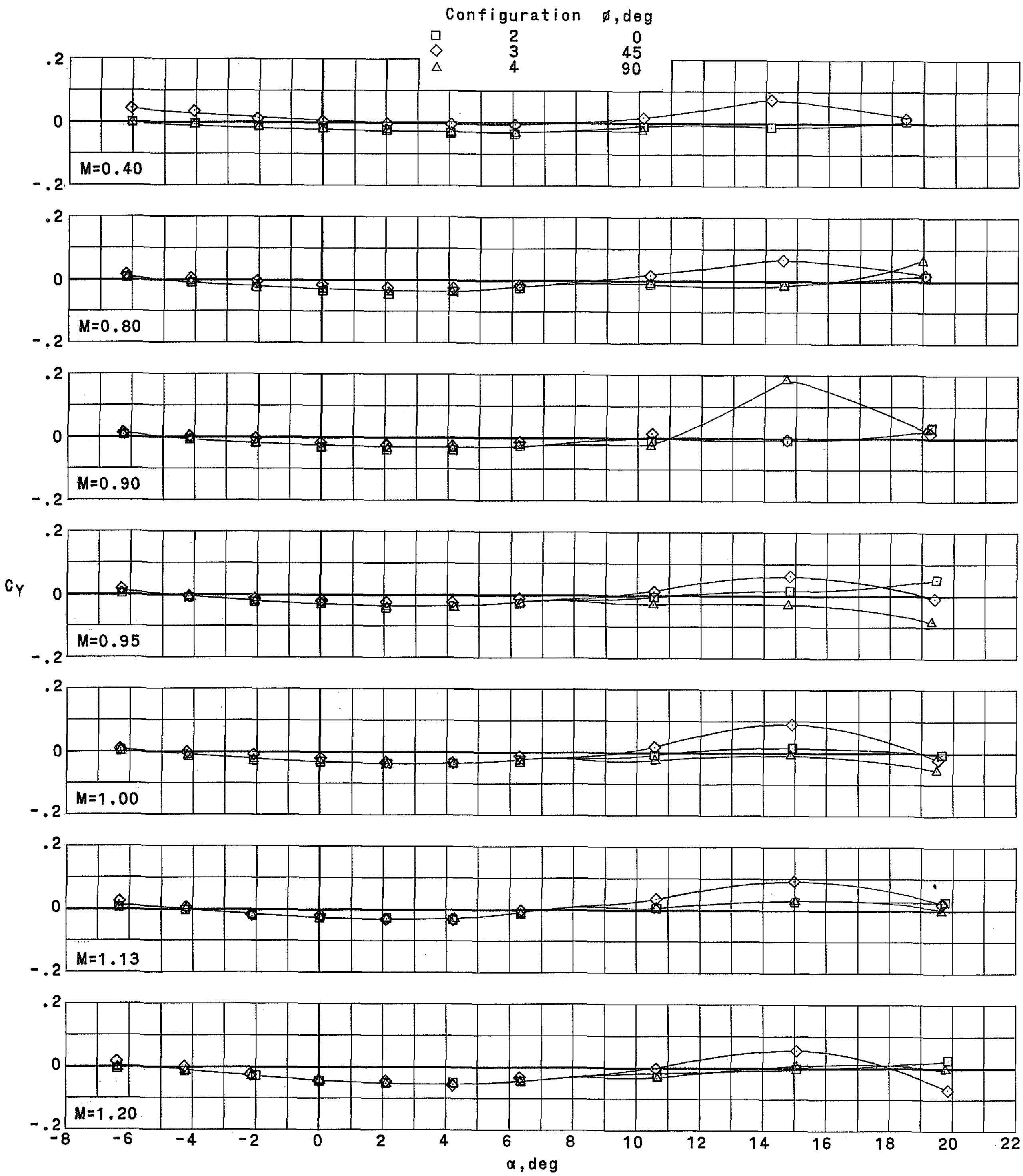

(f) Side-force coefficient.

Figure 7.- Concluded.

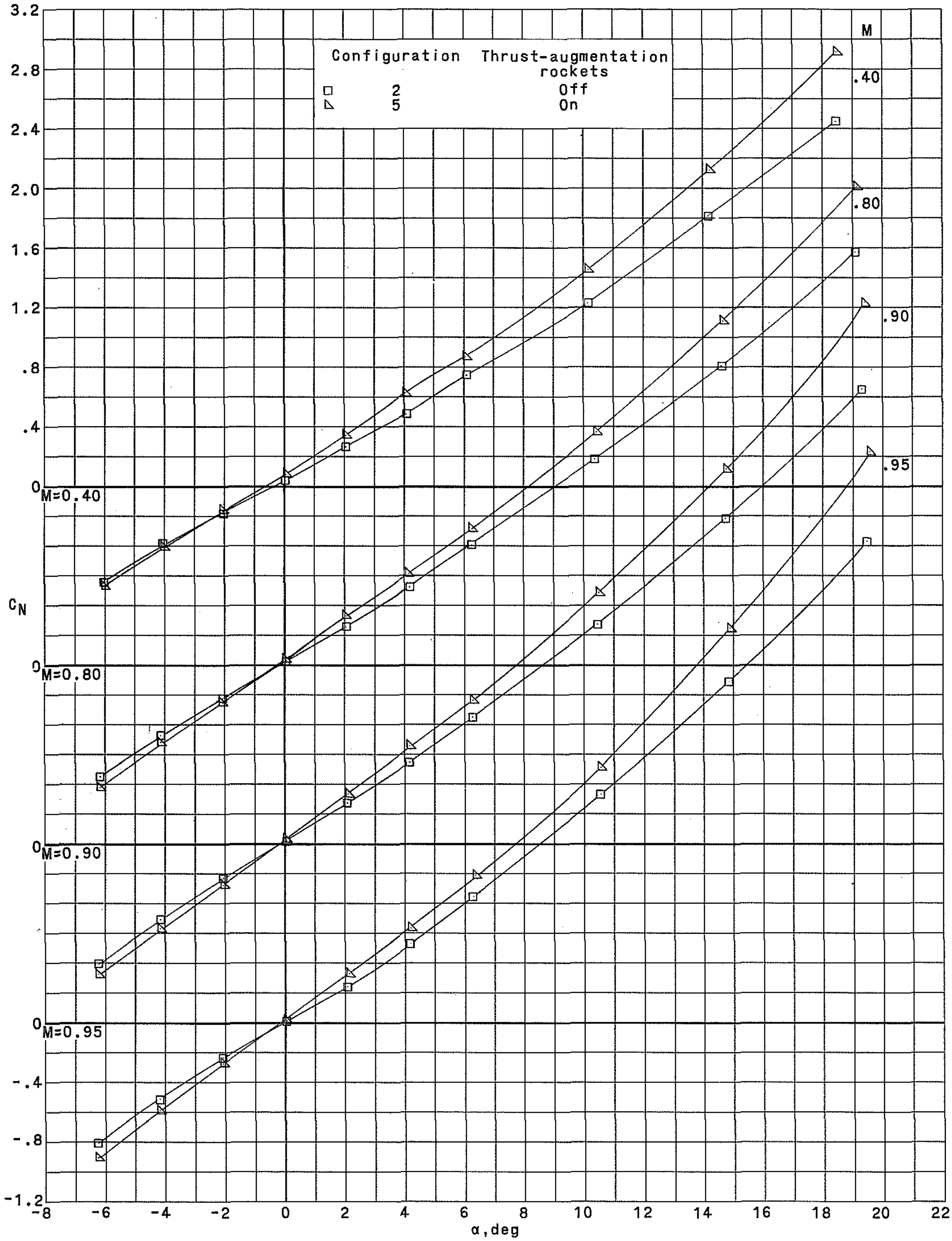

(a) Normal-force coefficient.

Figure 8.- Static aerodynamic characteristics of configurations 2 and 5. Thrust-augmentation-rockets effects.

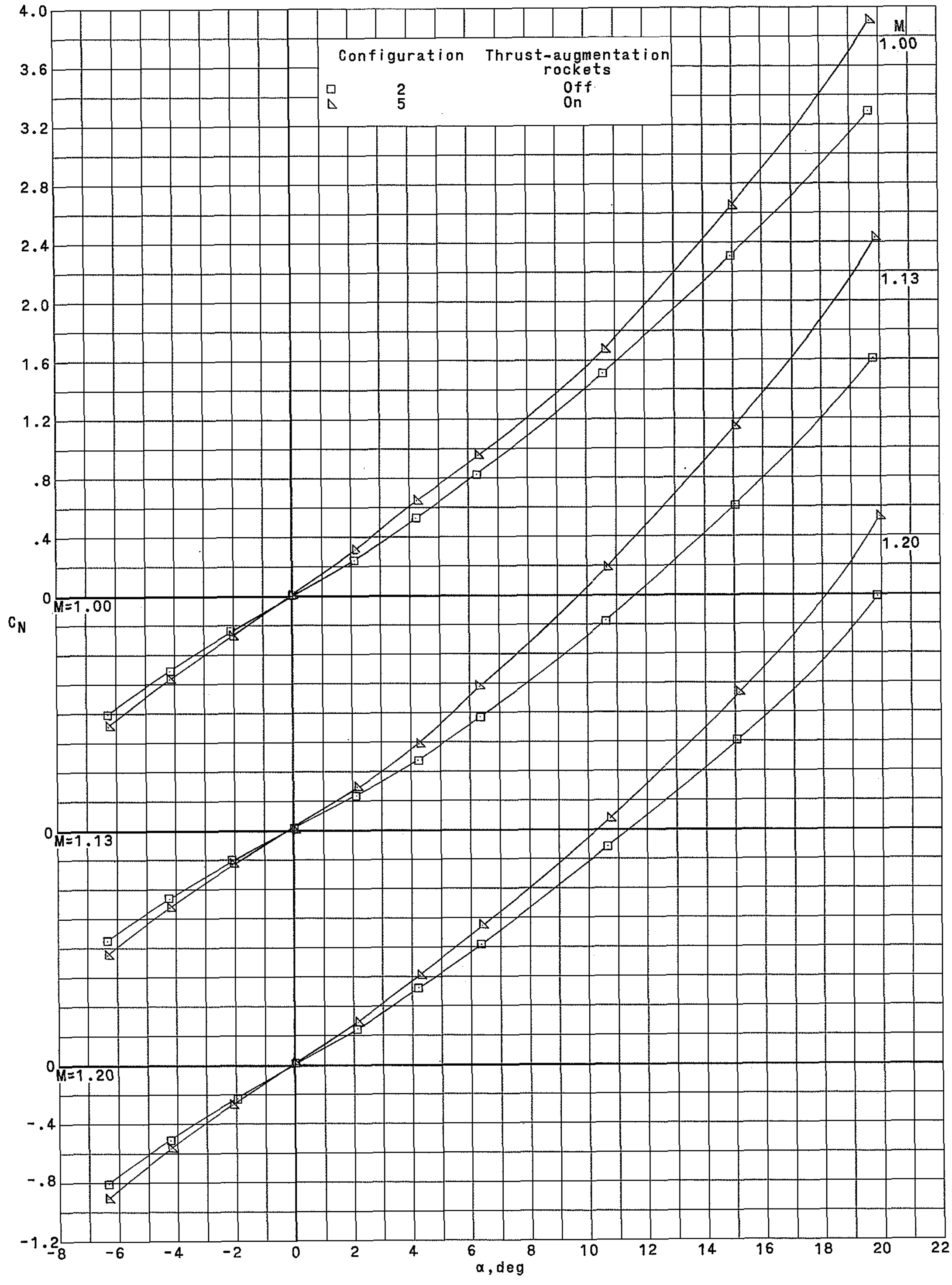

(a) Normal-force coefficient. Concluded.

Figure 8.- Continued.

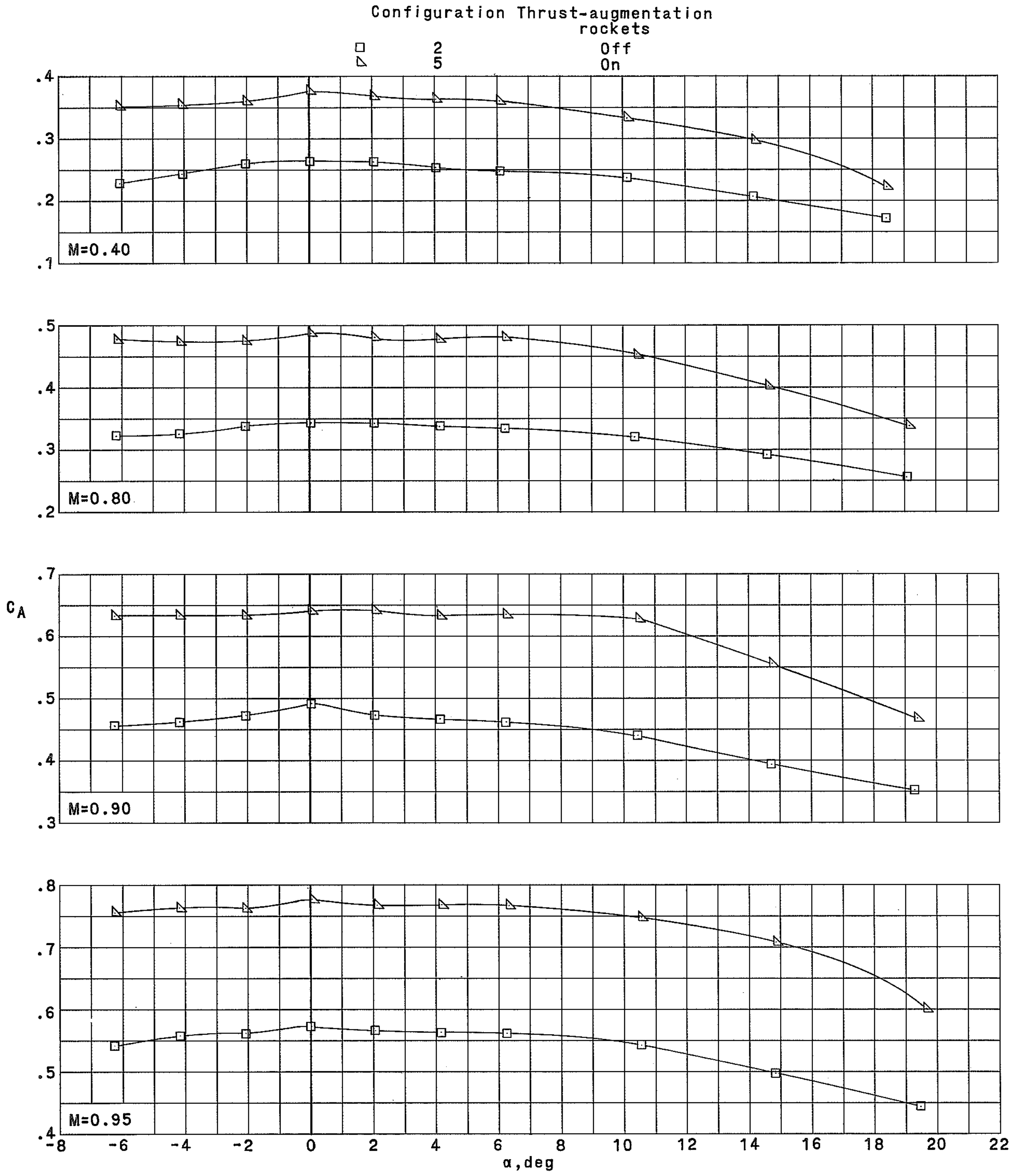

(b) Axial-force coefficient.

Figure 8.- Continued.

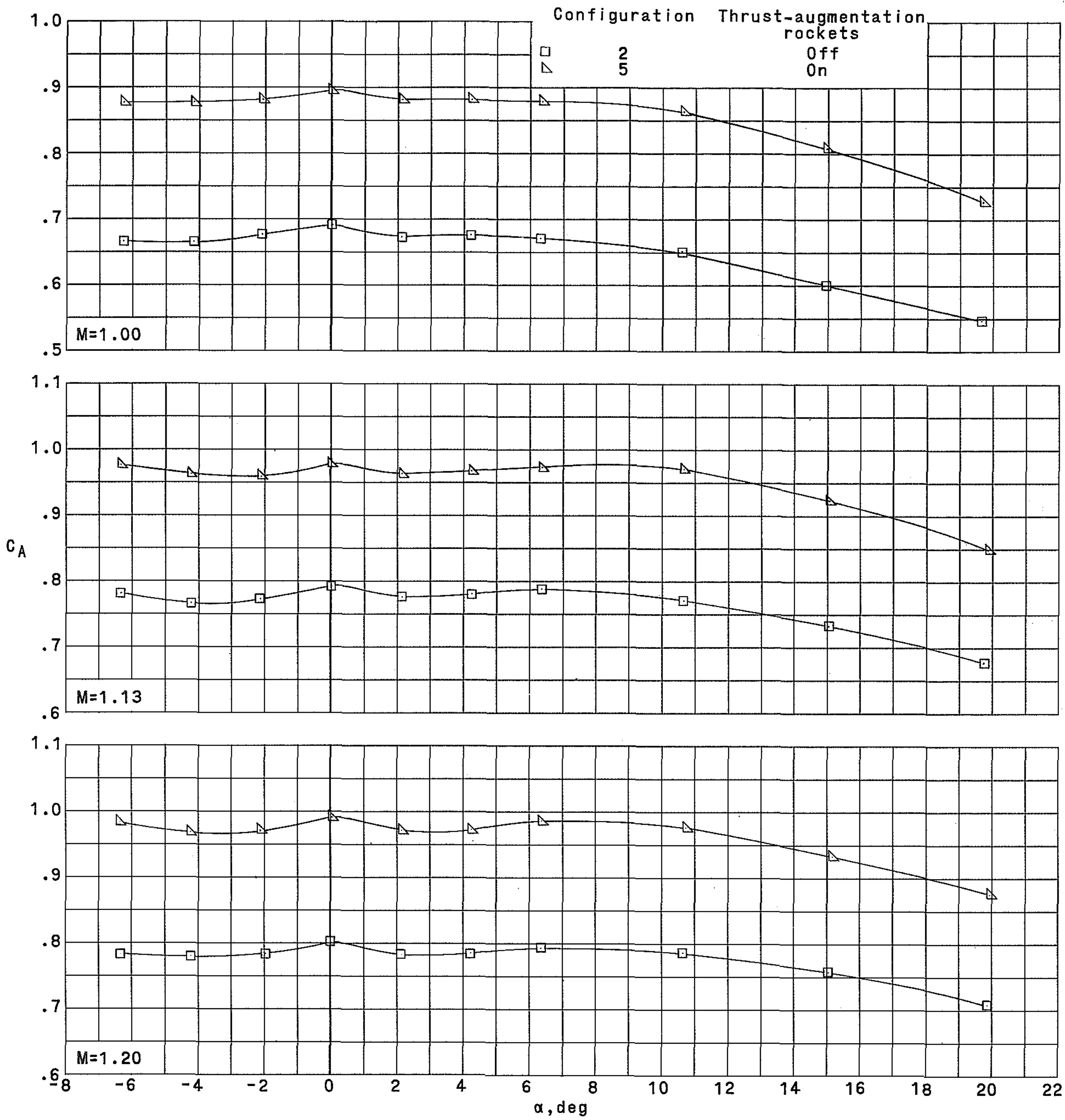

(b) Axial-force coefficient. Concluded.

Figure 8.- Continued.

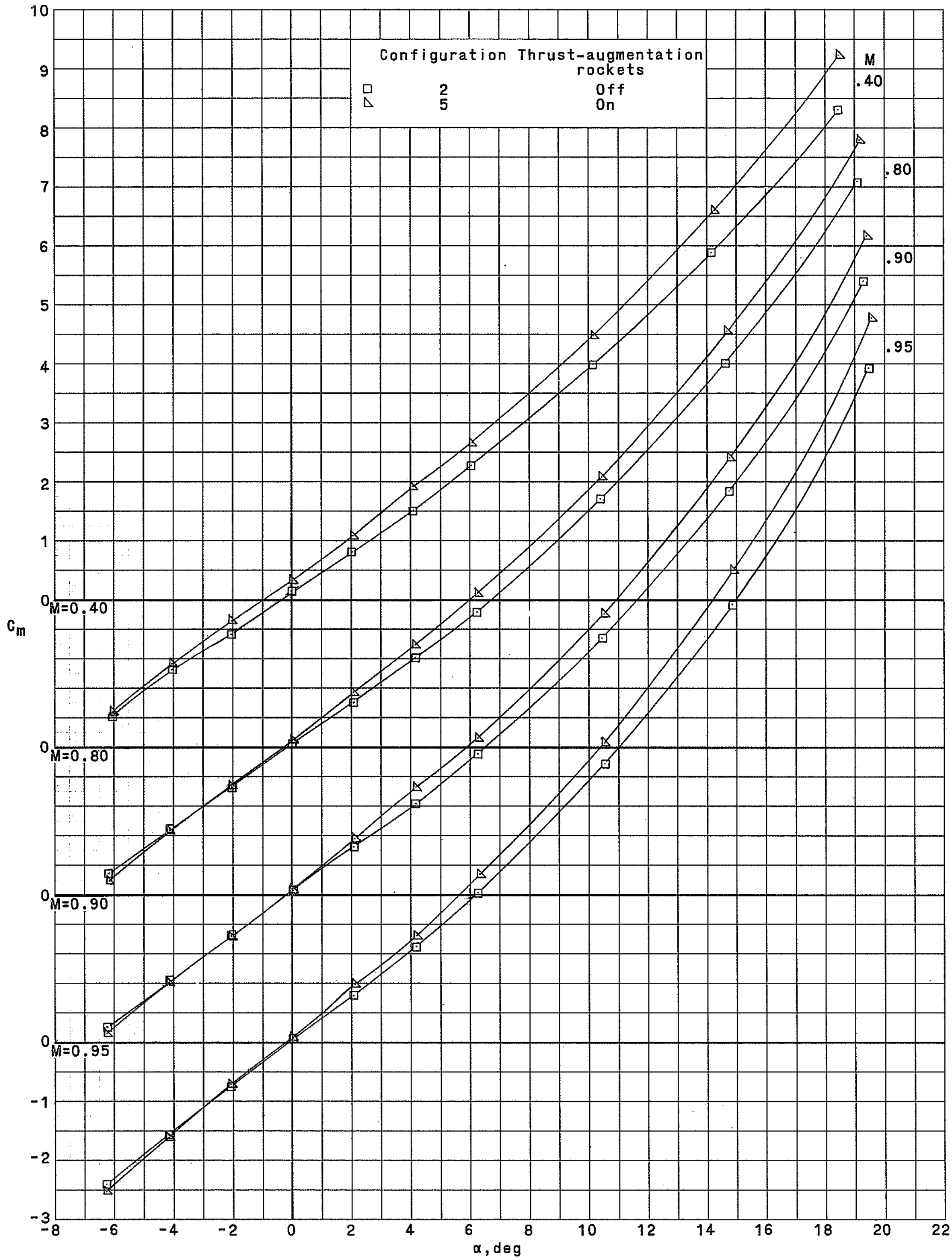

(c) Pitching-moment coefficient.

Figure 8.- Continued.

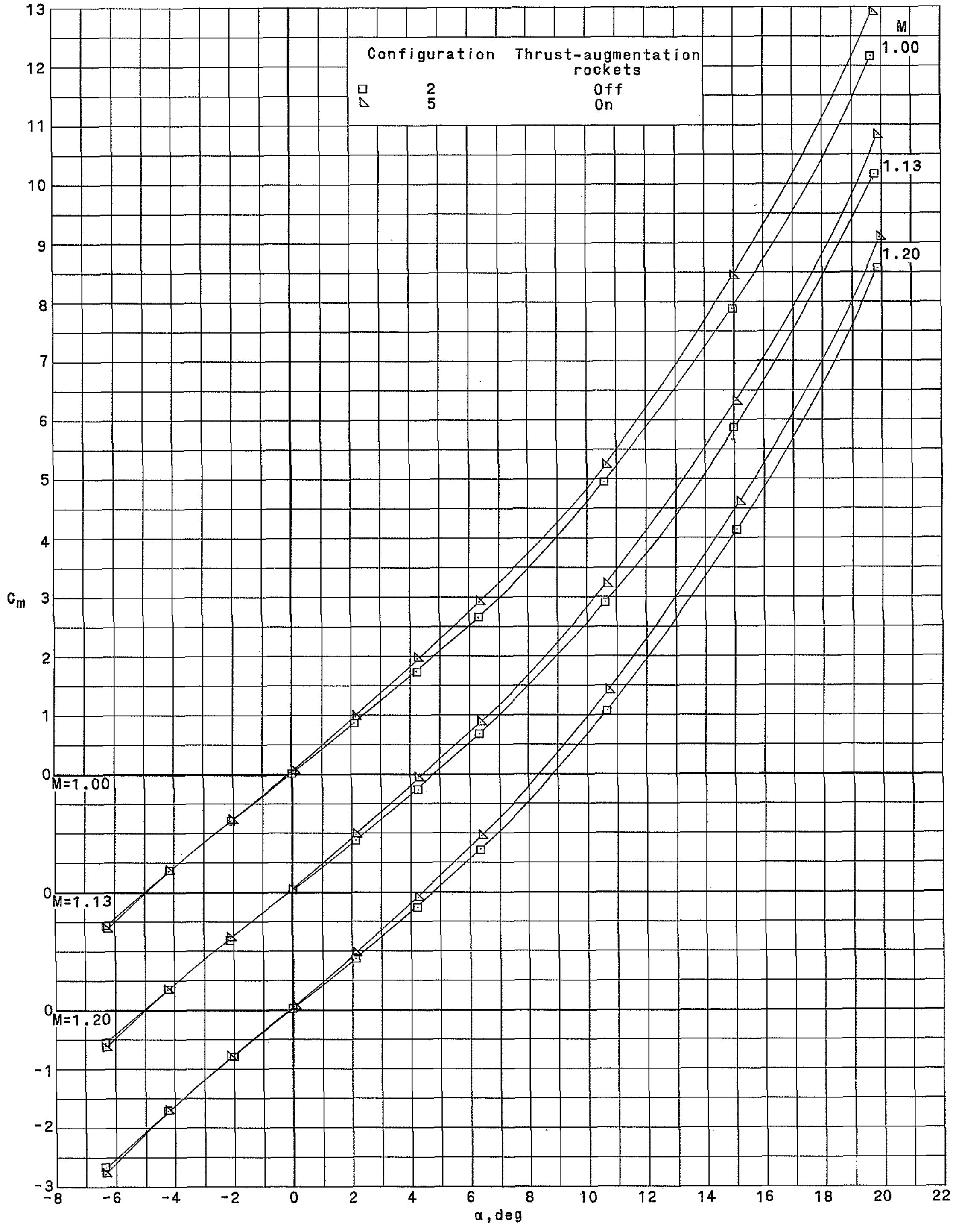

(c) Pitching-moment coefficient. Concluded.

Figure 8.- Continued.

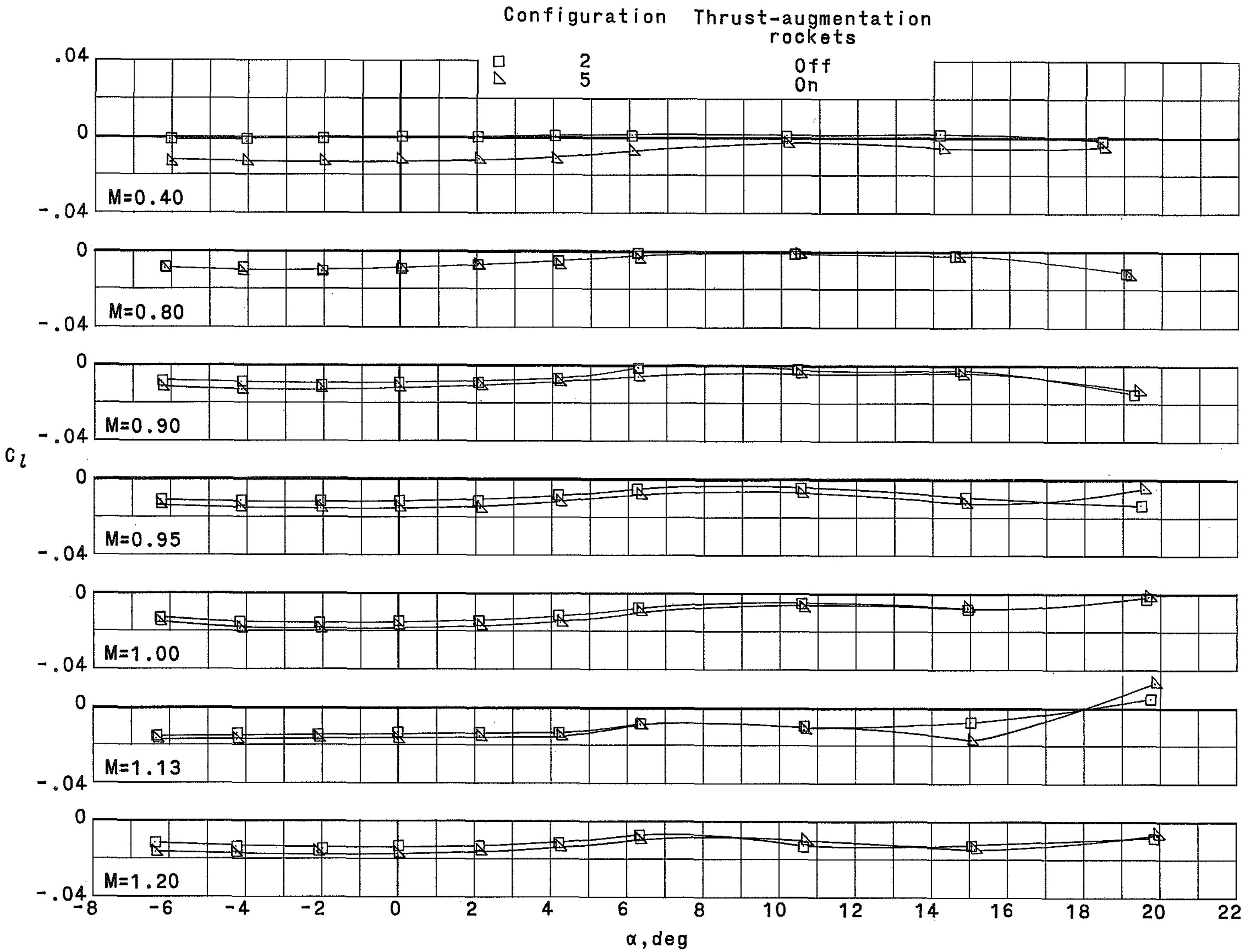

(d) Rolling-moment coefficient.

Figure 8.- Continued.

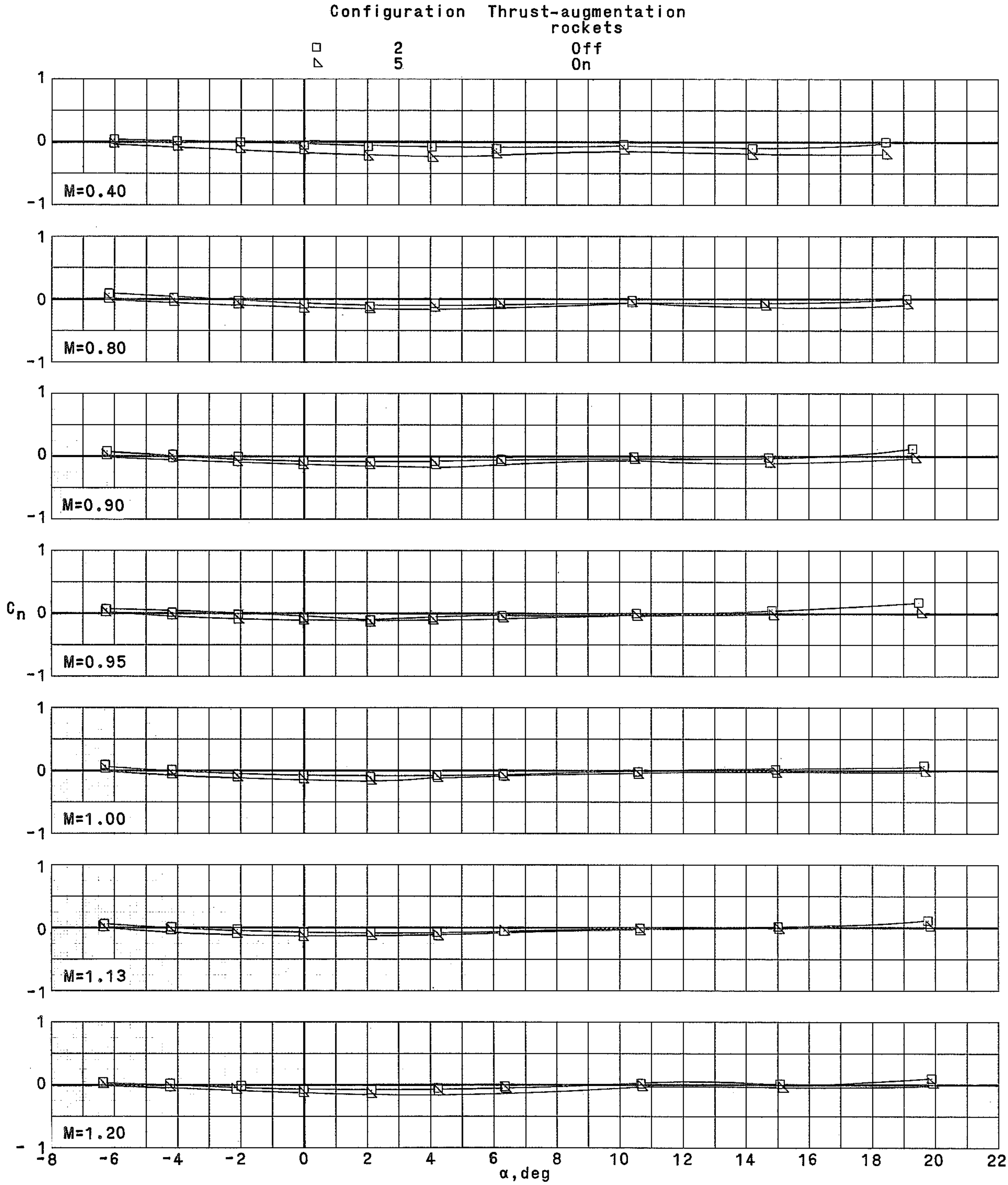

(e) Yawing-moment coefficient.

Figure 8.- Continued.

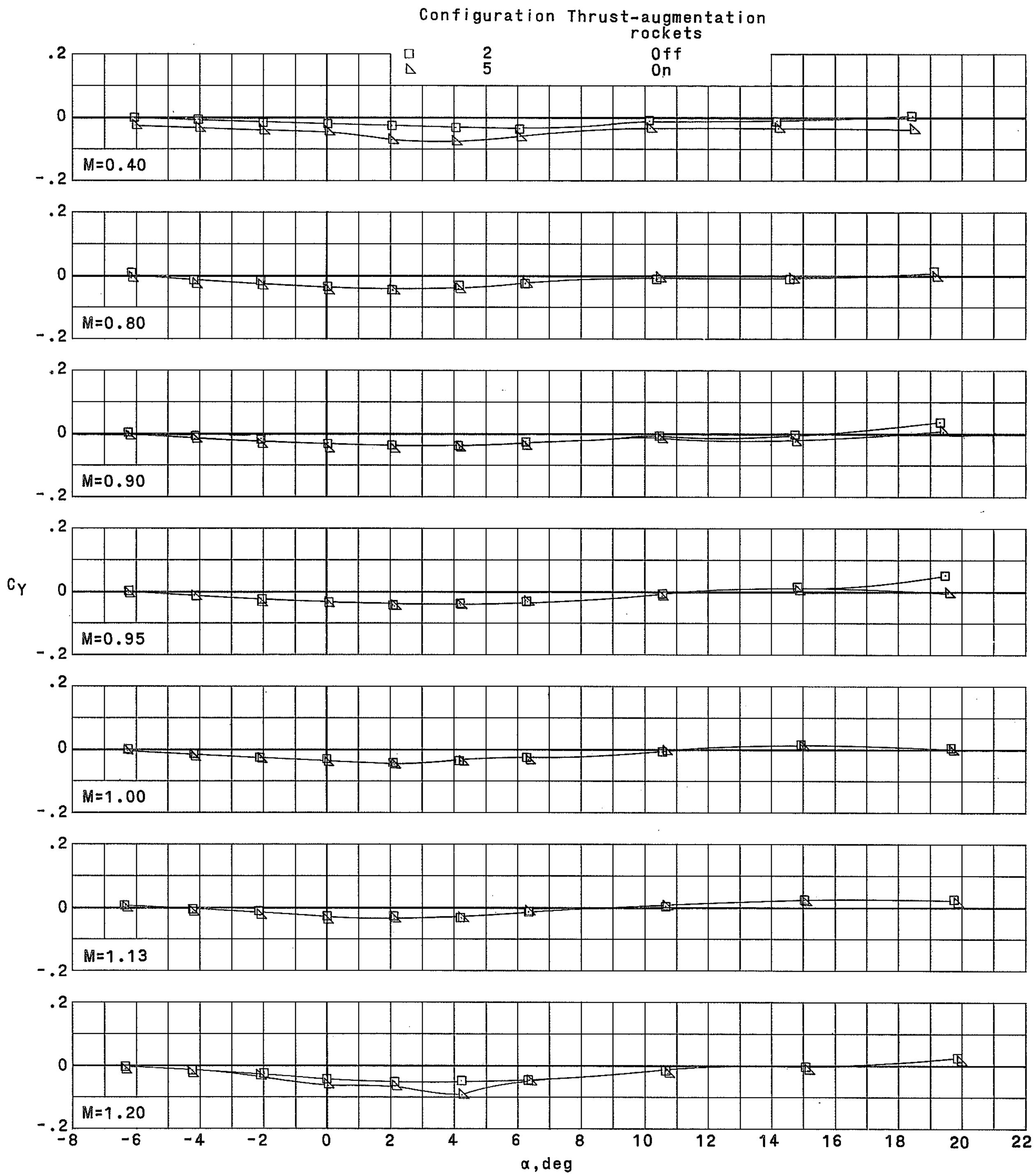

(f) Side-force coefficient.

Figure 8.- Concluded.

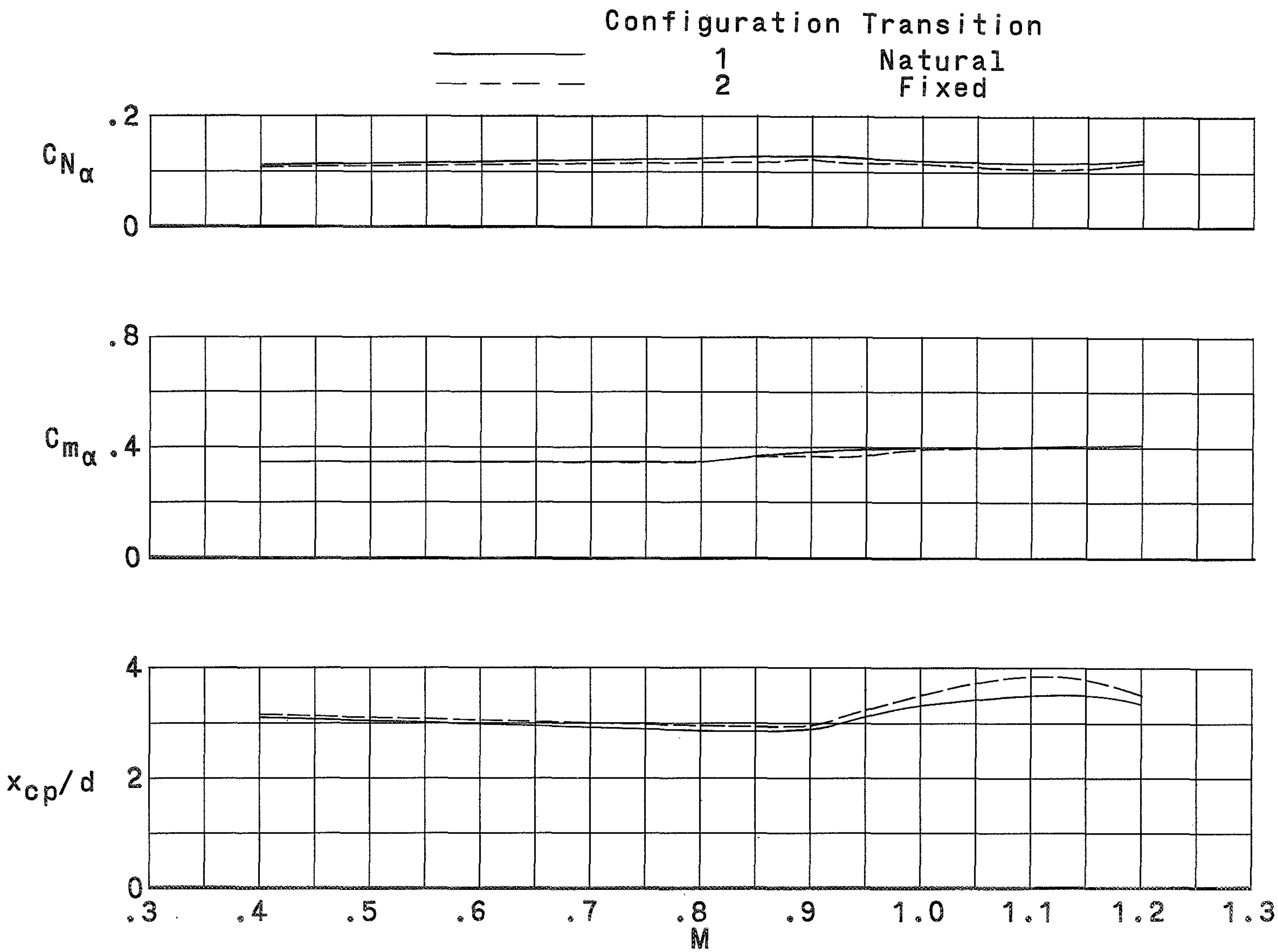

(a) Slope of normal-force curve, slope of pitching-moment curve, and center-of-pressure location for configurations 1 and 2. Transition effects.

Figure 9.- Summary of static longitudinal aerodynamic characteristics at $\alpha = 0^o$.

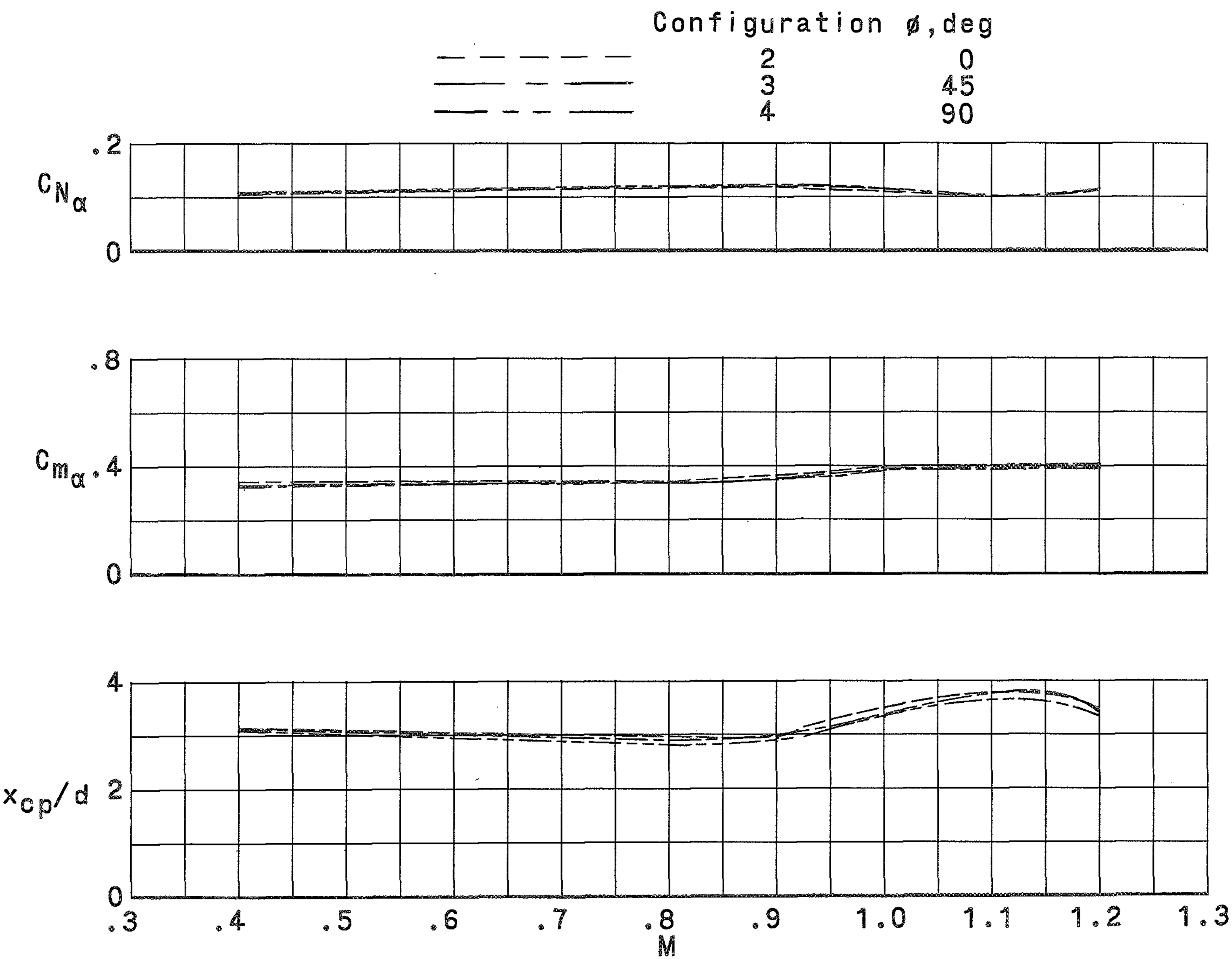

(b) Slope of normal-force curve, slope of pitching-moment curve, and center-of-pressure location for configurations 2, 3, and 4. Roll-angle effects.

Figure 9.- Continued.

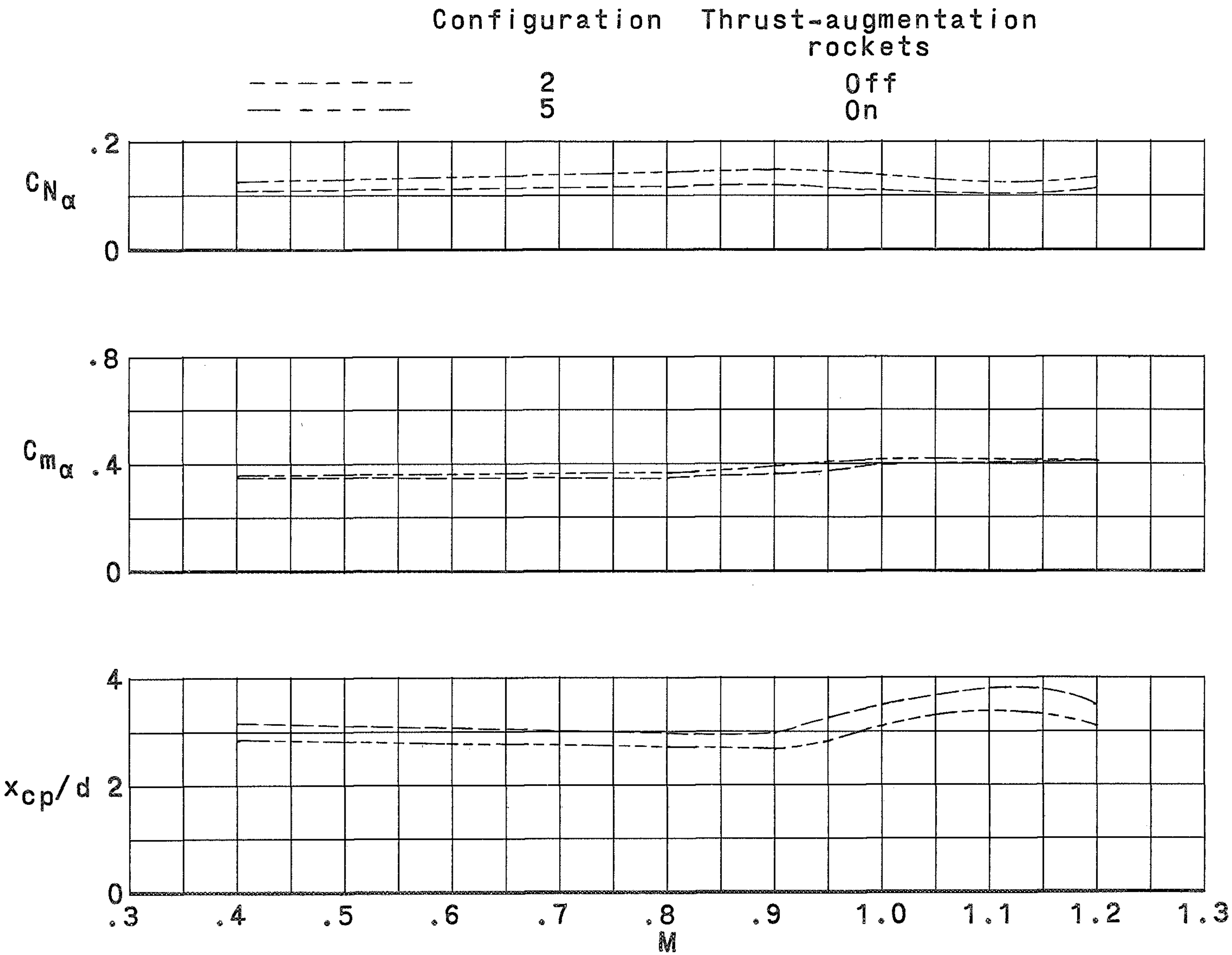

(c) Slope of normal-force curve, slope of pitching-moment curve, and center-of-pressure location for configurations 2 and 5. Thrust-augmentation-rockets effects.

Figure 9.- Continued.

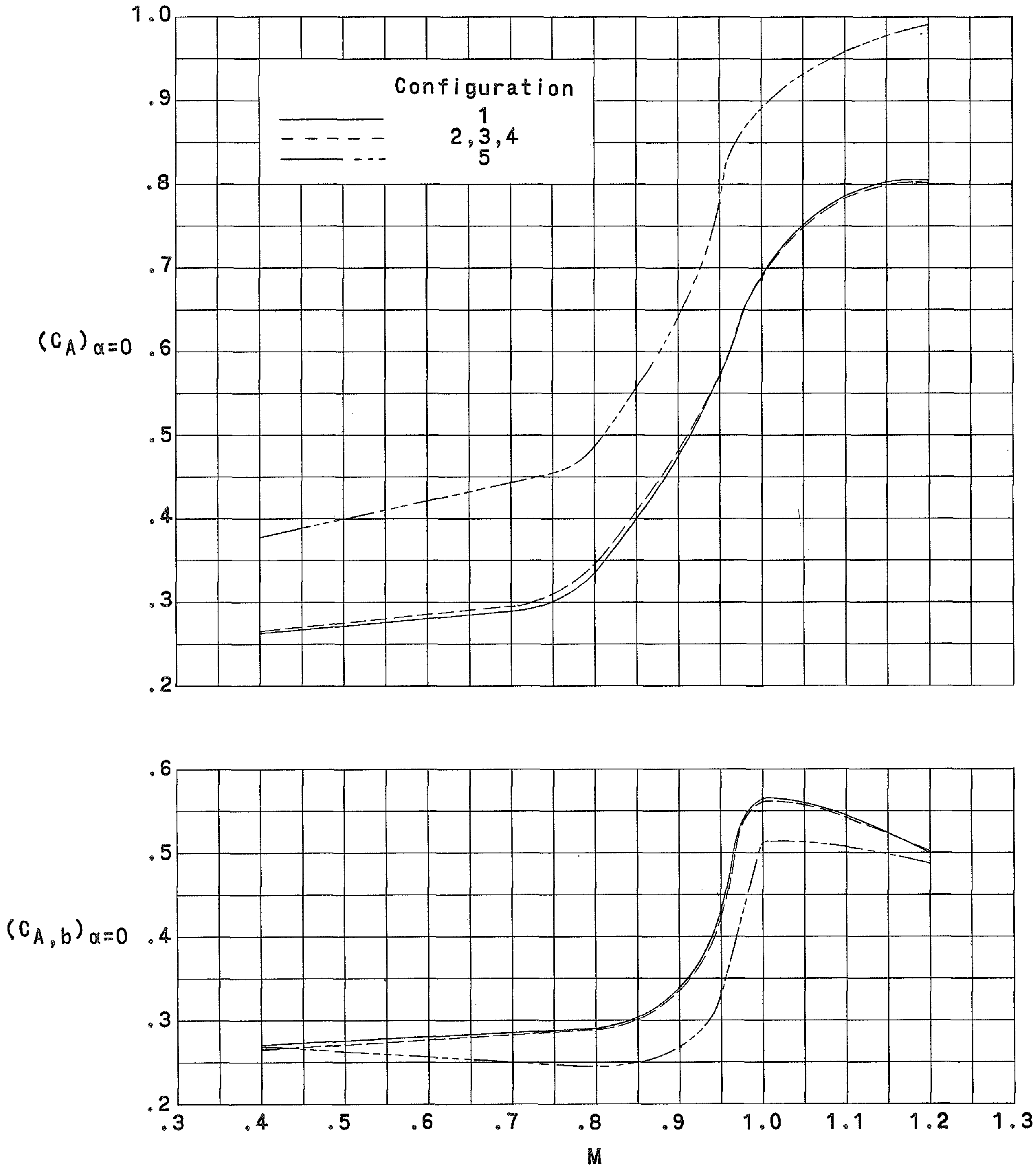

(d) Axial-force coefficient and base + axial-force coefficient for all configurations.

Figure 9.- Concluded.

NASA-Langley, 1969 —— 31 L-6615

NATIONAL AERONAUTICS AND SPACE ADMINISTRATION
WASHINGTON, D.C. 20546

OFFICIAL BUSINESS

FIRST CLASS MAIL

POSTAGE AND FEES PAID
NATIONAL AERONAUTICS AND
SPACE ADMINISTRATION

POSTMASTER: If Undeliverable (Section 158 Postal Manual) Do Not Return

"The aeronautical and space activities of the United States shall be conducted so as to contribute . . . to the expansion of human knowledge of phenomena in the atmosphere and space. The Administration shall provide for the widest practicable and appropriate dissemination of information concerning its activities and the results thereof."

—NATIONAL AERONAUTICS AND SPACE ACT OF 1958

NASA SCIENTIFIC AND TECHNICAL PUBLICATIONS

TECHNICAL REPORTS: Scientific and technical information considered important, complete, and a lasting contribution to existing knowledge.

TECHNICAL NOTES: Information less broad in scope but nevertheless of importance as a contribution to existing knowledge.

TECHNICAL MEMORANDUMS: Information receiving limited distribution because of preliminary data, security classification, or other reasons.

CONTRACTOR REPORTS: Scientific and technical information generated under a NASA contract or grant and considered an important contribution to existing knowledge.

TECHNICAL TRANSLATIONS: Information published in a foreign language considered to merit NASA distribution in English.

SPECIAL PUBLICATIONS: Information derived from or of value to NASA activities. Publications include conference proceedings, monographs, data compilations, handbooks, sourcebooks, and special bibliographies.

TECHNOLOGY UTILIZATION PUBLICATIONS: Information on technology used by NASA that may be of particular interest in commercial and other non-aerospace applications. Publications include Tech Briefs, Technology Utilization Reports and Notes, and Technology Surveys.

Details on the availability of these publications may be obtained from:

SCIENTIFIC AND TECHNICAL INFORMATION DIVISION

NATIONAL AERONAUTICS AND SPACE ADMINISTRATION

Washington, D.C. 20546